UNIVERSITÀ
DEGLI STUDI
DI PADOVA

DIPARTIMENTO
DI INGEGNERIA
DELL'INFORMAZIONE

DIPARTIMENTO DI INGEGNERIA DELL'INFORMAZIONE

CORSO DI LAUREA MAGISTRALE IN BIOINGEGNERIA INDUSTRIALE

INNOVATIVE STRATEGIES FOR DRUG TESTING AND MYCOTOXIN CYTOTOXICITY EVALUATION: THE CONVERGENCE OF MICROFLUIDIC DEVICES AND 3D CULTURE SISTEMS

Relatore: Prof. Elisa Cimetta

Laureando: Massimiliano Pamio

ANNO ACCADEMICO 2023 – 2024

Data di laurea 04/04/2024

Abstract

Standard *in vitro* experimental models have proven invaluable in advancing our knowledge of biological systems for decades, despite being affected by several limitations. With a focus on cancer research, we highlight their poor mimic of the complexity and heterogeneity of human tumors and scarce control over the microenvironment spatial-temporal composition.

Technological advances in bio- and microfabrication are revolutionizing cancer research by providing tools more closely recapitulating the complex three-dimensional (3D) architecture and environment of native tumors compared to traditional two-dimensional (2D) cell cultures. The integration of 3D models with microfluidic technologies enables further control of the spatial and temporal dynamics of *in vivo* tumor microenvironments.

We set two main goals for this proposed research: assessing the toxicological risks of mycotoxins and conducting drug tests on human cancer models. To this aim, we will design, produce, and validate two microfluidic platforms. The first is dedicated to investigating cytotoxicity induced by mycotoxins, while the second focuses on assessing cytotoxicity induced by a chemotherapeutic drug while increasing the experimental throughput by generating different drug concentrations within the same device.

The first microfluidic platform is called SpheroFlow Device (SFD) and aimed to evaluate the cytotoxic effects induced by exposure to a series of mycotoxins of food origin on human Neuroblastoma (NB) cells. Mycotoxins, secondary metabolites found in numerous food products, have been associated with chronic and acute health effects upon human and animal exposure. For our investigation, spheroids were obtained and characterized from a NB cell line (SH-SY5Y). Subsequently, these spheroids were transferred to the microfluidic device specially designed and fabricated in PDMS through the replica molding process. The spheroids were then exposed to various concentrations of mycotoxins for different time intervals using a pump connected to the device. Following the mycotoxin treatment, analyses were conducted on the spheroids to assess their viability.

The second microfluidic platform, named MicroGradient Generator (MGG), can create 5 different concentrations of 5-Fluorouracil (5FU), a chemotherapy drug frequently employed in cancer therapy. The platform was employed to test the drug on Colorectal Cancer (CRC) spheroids, formed using the HCT15 cell line. The microfluidic chip for drug testing was fabricated from PDMS via replica molding. The HCT15 spheroids were seeded into the microfluidic device, embedded in GelMA, a biocompatible and printable hydrogel. When

connected to a syringe pump, the samples could be exposed to the different drug concentrations generated by the device. Qualitative analyses were performed to evaluate the impact of different drug concentrations on CRC tumor spheroids.

The integration of microfluidic technology with 3D tumor models holds promise for advancing drug testing and toxicological studies, offering a more physiologically relevant approach to understanding the effects of various compounds on tumor cells.

Riassunto

I modelli sperimentali standard *in vitro* hanno dimostrato di essere inestimabili nel progresso della nostra conoscenza dei sistemi biologici per decenni, nonostante siano affetti da diverse limitazioni. Con un focus sulla ricerca sul cancro, sottolineiamo la loro scarsa capacità di mimare la complessità e l'eterogeneità dei tumori umani e il limitato controllo sulla composizione spazio-temporale del microambiente. I progressi tecnologici nella bio- e microfabbricazione stanno rivoluzionando la ricerca sul cancro fornendo strumenti che ricreano più fedelmente l'architettura tridimensionale (3D) e l'ambiente dei tumori nativi rispetto alle tradizionali colture cellulari bidimensionali (2D). L'integrazione di modelli 3D con tecnologie microfluidiche consente un ulteriore controllo della dinamica spazio-temporale dei microambienti tumorali *in vivo*. Gli obiettivi principali della ricerca proposta sono due: valutare i rischi tossicologici delle micotossine e condurre test di farmaci su modelli di cancro umano. A questo scopo, progetteremo, produrremo e convalideremo due piattaforme microfluidiche. La prima è dedicata all'indagine della citotossicità indotta dalle micotossine, mentre la seconda si concentra sull'analisi della citotossicità indotta da un farmaco chemioterapico, aumentando la capacità sperimentale generando diverse concentrazioni di farmaco nello stesso dispositivo. La prima piattaforma microfluidica si chiama SpheroFlow Device (SFD) e mira a valutare gli effetti citotossici indotti dall'esposizione a una serie di micotossine di origine alimentare su cellule di neuroblastoma umano (NB). Le micotossine, metaboliti secondari presenti in numerosi prodotti alimentari, sono state associate a effetti cronici e acuti sulla salute in seguito a esposizione umana e animale. Per la nostra indagine, sono stati ottenuti e caratterizzati sferoidi da una linea cellulare di NB (SH-SY5Y). Successivamente, questi sferoidi sono stati trasferiti al dispositivo microfluidico appositamente progettato e fabbricato in PDMS mediante il processo di replica molding. Gli sferoidi sono stati poi esposti a varie concentrazioni di micotossine per diversi intervalli di tempo utilizzando una pompa collegata al dispositivo. Dopo il trattamento con micotossine, sono state condotte analisi sugli sferoidi per valutare la loro vitalità. La seconda piattaforma microfluidica, chiamata MicroGradient Generator (MGG), è in grado di creare 5 diverse concentrazioni di 5-fluorouracile (5FU), un farmaco chemioterapico comunemente impiegato nella terapia del cancro. La piattaforma è stata impiegata per testare il farmaco su sferoidi di cancro del colon-retto (CRC), formati utilizzando la linea cellulare HCT15. Il chip microfluidico per i test di farmaci è stato fabbricato in PDMS tramite replica molding. Gli

sferoidi di HCT15 sono stati seminati nel dispositivo microfluidico, incorporati in GelMA, un idrogel biocompatibile e stampabile. Collegando il dispositivo a una pompa siringa, i campioni potevano essere esposti alle diverse concentrazioni di farmaco generate dal dispositivo. Sono state eseguite analisi qualitative per valutare l'impatto delle diverse concentrazioni di farmaco sugli sferoidi tumorali di CRC.

L'integrazione della tecnologia microfluidica con i modelli tumorali 3D offre promette di far progredire la sperimetazione di farmaci e gli studi tossicologici, offrendo un approccio più fisiologicamente rilevante per comprendere gli effetti di vari composti sulle cellule tumorali.

Table of Contents

List of figures

List of tables

Chapter 1

State of the art

1.1 Microfluidics

Microfluidics is the science of manipulating and controlling fluids and particles at micron and submicron dimensions. This enables precise fluid control through micro-scale devices, utilizing technologies initially pioneered by the semiconductor industry and later advanced by the micro-electromechanical systems (MEMS) field.
Microfluidic devices facilitate complete analysis in a single platform (lab-on-a-chip), with their reduced dimensions allowing to easier manipulation of small amount of product compared to traditional methods.
Over the past two decades, microfluidics technologies have evolved into sophisticated platforms where unit operations like valves, mixers, and pumps are implemented for better control of the fluid. Microfluidics goes beyond handling small volumes; it ensures continuous and parallel fluid processing, leading to[1]:

- Improved automation
- Potential attainment of steady-state conditions
- Increased throughput
- Enhanced efficiency
- Reduced experimental time
- Lower total cost of experiments

The fluid phenomena that dominate liquids at this length scale are significantly different from those at the macro-scale[2]. For example, the relative effect of the force produced by gravity at micro-scale dimensions is greatly reduced compared to its dominance at the macro-scale[3]. This and other properties find practical use in diverse fields spanning from protein crystallization, clinical and forensic analysis, separation operations and proteomics, to the development of micropumps, fuel cells, and molecular diagnostics tools[2].

1.1.1 Physics of microfluidics

As anticipated in §1.1, the governing phenomena at the micro-scale are different from those of the macro-scale. The analysis of fluid profiles when confined in microfluidic results in predominantly laminar flows[4]. This laminar flow allows for precise mass transport calculations over time. With stable fluid streamlines and primary mixing occurring through diffusion, the dominant transport mechanism is diffusion, often overlooked in other systems. The high area-volume ratio further emphasizes surface effects over volumetric ones, leading viscous and tensile forces to surpass inertia forces[5].

The motion of a Newtonian fluid is described by the Navier-Stokes equation, reported in 1.1:

$$\rho \frac{D\,(v)}{Dt} = \rho\left(\frac{\partial v}{\partial t} + (v \cdot \nabla)v\right) = \mu\nabla^2(v) - \nabla P + \rho g \qquad (1.1)$$

On the right side, the term is formed by the sum of the velocity variation over time and the convective term, representing the substantial derivative of the velocity vector v [m/s]. On the left, we find the diffusion term, pressure [Pa], and gravity forces [m/s²]. As mentioned above, in microfluidic systems, viscous forces outweigh inertial forces, allowing to neglect the convective term $(v\cdot\nabla)v^2$.

In microfluidics, dimensionless numbers (summarized in Table 1.1) are often calculated to compare phenomena or length scales and are thus an important tool for a quick and immediate understanding of the dominant forces and fluid behavior.

Table 1.1 *Dimensionless numbers used in microfluidics. Adapted from*[1].

Acronym	Name	Phenomena compared
Re	Reynolds	Inertial/viscous
Pe	Péclet	Convection/diffusion
Ca	Capillary	Viscous/interfacial
Wi	Weissenberg	Polymer relaxation time/shear rate time
De	Deborah	Polymer relaxation time/flow time
El	Elasticity	Elastic effects/inertial effects
Gr	Graschof	Re for buoyant flow
Ra	Rayleigh	Pe for buoyant flow
Kn	Knudsen	Slip length/macroscopic length

The Reynolds number (Re; Equation 1.2), comparing inertial and viscous forces, serves as the criterion for distinguishing between laminar and turbulent flow regimes.

$$Re \equiv \frac{\rho v D}{\mu} \tag{1.2}$$

The fluid density, denoted as ρ and typically measured in [kg/m³], is a key factor in fluid dynamics. The characteristic velocity of the fluid, represented by v in [m/s], along with the fluid viscosity (μ) in [Pa·s], and the pipe diameter (D), contribute to defining Re. In cases where the pipe is non-tubular, the equivalent diameter (D_{eq}) is calculated using Equation 1.3:

$$D_{eq} \equiv \frac{4S}{2P} \tag{1.3}$$

where S is the area available for the passage of the fluid [m^2] and P is the semi-perimeter [m]. In a tubular pipe, for Re < 2300 the fluid is in a laminar regime while for Re > 2300 the flow is turbulent, thus characterized by the presence of eddies leading to instability and unpredictability.

Generally, in microfluidic systems, due to the small dimensions, the fluid behaves in a laminar way[5] which is highly predictable and allows to simplify the Navier-Stokes and the mass transport balance equations. Under this assumption, Equation 1.1 can be easily solved, obtaining the Hagen Poiseuille equation (Equation 1.4):

$$v = 2V\left(1 - \frac{r^2}{R^2}\right) \tag{1.4}$$

V represents the ratio of volumetric flow rate to cross-sectional area [m/s], and R is the radius of the pipe [m]. The outcome is illustrated in Figure 1.1: the velocity profile exhibits a parabolic pattern, reaching its maximum value $v_{max} = 2V$ in $r = 0$, while $v = 0$ at the wall $r = R$.

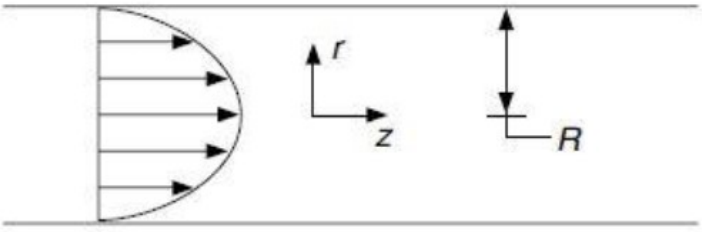

Figure 1.1 *Velocity profile for a laminar flow in a pipe. Adapted from*[6].

Another crucial dimensionless factor is the Péclet number (Pe), serving as a metric for the balance between convection and diffusion in mass transport phenomena. Its definition is articulated in Equation 1.5:

$$Pe \equiv \frac{vD}{D_i} \tag{1.5}$$

where v is the velocity inside the pipe [m/s], D is the pipe diameter [m], and D_i is the diffusion coefficient of the species i [m^2/s]. The coefficient *Di* can be determined using the Einstein-Smoluchowski equation (Equation 1.6):

$$D_i = \eta k_B T \tag{1.6}$$

Under the assumption of spherical particle movement in a viscous fluid, the Einstein-Smoluchowski equation transforms into the Stokes-Einstein equation (Equation 1.7), where η is the particle mobility [kg/s], k_B is the Boltzmann constant [J/K], and T is the temperature [K]:

$$D_i = \frac{k_B T}{6\pi\mu r} \tag{1.7}$$

where *r* is the radius of the particles [m]. Consequently, a small Pe value, typically ranging between 0.05 and 500, signifies a substantial influence of the diffusion term. Conversely, for a high Pe value, approximately 10^3, convection becomes the predominant transport mechanism. In microfluidic systems characterized by laminar flow without eddies, mass transport primarily relies on the diffusion mechanism, leading to low mixing.
Considering now the conservation equation of species i (Equation 1.8):

$$\frac{dC_i}{dt} = -\nabla(C_i v) - \nabla(J_i) + R_i \tag{1.8}$$

On the left side is the variation of concentration of *i* along time, while on the right side are the convective and diffusion fluxes, along with the reaction term. The diffusive flux [mol/m²s] can be expressed through the Fick law (Equation 1.9):

$$J_i = -D_i \nabla(C_i) \tag{1.9}$$

In microfluidic devices, as mentioned earlier, the convection term is insignificantly small compared to the diffusion term. Additionally, under the assumption of attaining a steady state and the absence of any reactions, Equation 1.8 can be streamlined in Equation 1.10:

$$0 = D_{m,i} \nabla^2(C_i) \tag{1.10}$$

Concluding, the final significant dimensionless number is the Capillary number (Ca), defined as (Equation 1.11):

$$Ca = \frac{\mu v}{\gamma} \tag{1.11}$$

Ca relates the viscous forces with the surface tension, playing a crucial role in immiscible fluids. In this case surface tension influences the dynamics of the free surface[2], where μ is the fluid viscosity [Pa·s], v is the velocity inside the channel [m/s], and γ is the surface tension of the fluid [N/m], typically with air.

1.1.2 Microfluidic devices: materials and technology

After an overview of the physics of microfluidics, focused on the laminar flows and short transport distances, we now discuss the choices of the materials and the specific fabrication techniques. A proper evaluation and correct selection of both is what could truly enable to obtain a powerful tool to realize highly sensitive, high speed, high throughput, and low-cost analyses[6].

1.1.2.1 Materials

The material choice for the microdevice is determined by chemical and biological considerations. This involves determining the technical characteristics (such as optical transparency, permeability to gas exchanges, and biocompatibility) that the chip must possess to perform a specific task.

Initially, materials used for microfluidic applications were silicone and glass[7], but over the years there has been a transition from the use of glass to a more marked use of polymeric materials.

Fabrication with silicon[8] and glass needs similar methods, either subtractive (e.g., wet or dry etching) or additive, such as metal or chemical vapor deposition, to create structures. Silicon was first selected due to its resistance to organic solvents, ease in metal depositing and high thermal conductivity. However, its handling is not easy due to its hardness, which complicates the creation of active microfluidic components like valves and pumps. Additionally, it is transparent to infrared but not to visible light, posing challenges for typical fluorescence detection or fluid imaging in embedded structures. To address this issue, a solution is to have a transparent material (polymer or glass) bound to silicon in a hybrid system.

Given the long tradition of glass processing in chemical and biomedical laboratories, it is not surprising that the most used material for microfluidic chips over the years has been glass. Glass is an amorphous material with excellent optical properties, being transparent and resistant to chemical reagents, as well as electrically insulating[8]. Typically, two techniques are used to produce microfluidic devices in glass: photolithography and etching, wet or dry. Although well established, they are not suitable for mass production which makes glass a rather niche material for microfluidics. In fact, from an engineering point of view, it is preferable to look at other materials such as polymers and other techniques such as injection molding, which are more prone to mass production. However, in some cases it may be economically more advantageous to build small quantities of glass devices, rather than having to design and build molds suitable for the processing techniques of polymeric materials.

Polymers are organic-based, long-chain materials that have gained significant importance in microfluidics in the last years. The wide range of polymers offers great flexibility in choosing suitable materials with specific properties[8].

Compared to silicone and glass, polymers have the advantage of being inexpensive and easily accessible. This makes them the best materials for rapid prototyping and mass production, consequently becoming the most widely used for the construction of microfluidic chips nowadays. Figure 1.2 shows an example of a polymeric microfluidic chip.

The most widely used polymeric material in the field of microfluidics is polydimethylsiloxane (PDMS). PDMS is preferred many times over other materials due to its numerous advantages, such as elasticity, low toxicity, optical transparency, chemical inertness, low cost and rich permeability to gases, which can be advantageous for oxygen and carbon dioxide transport in

cell studies[9]. Despite the considerable number of advantages, an increasing number of scientific reports have begun to raise awareness on the potential negative effects associated with culturing and studying cells in PDMS microdevices[10]. PDMS, for instance, faces limitations due to material aging and inadequate chemical compatibility with numerous organic solvents. Additionally, it tends to absorb small molecules on its surface and accumulates water vapor during experiments. Moreover, PDMS chips are unsuitable for high-pressure operations, as they may alter the geometry of the microchannels.
However, these flaws do not prevent it from still being the most widely used material in microfluidic chip fabrication and the ones used in this work.

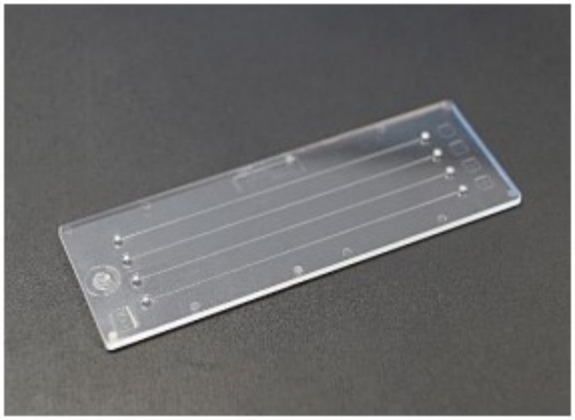

Figure 1.2 *Example of polymeric microfluidic chip. Adapted from*[8].

1.1.2.2 Production techniques

Photolithography and soft lithography are the two most widely adopted techniques to produce microfluidic devices.
Photolithography is a process that transfers shapes from a photomask to the surface of a silicon wafer using light. The protocol requires many steps and several different tools and chemicals[11]. Initially, a silicon wafer is chemically treated to remove contaminants[11] and humidity. Silicon dioxide is deposited as a barrier layer, and an adhesion promoter is added. The wafer is coated with photoresist by spin coating[12], either wet or dry, and solvent removal is done through soft baking. The next step, the crucial one, is aligning the mask with the wafer so that the individual areas of the photoresist are selectively exposed to optical or UV light. A mask, which looks like the chip, is a square glass plate or a film with holes or transparencies that allow light to shine through in a defined pattern[11]. The photomask is patterned depending on the choice of the photoresist: positive resins become more soluble upon UV exposure, while negative photoresist undergoes polymerization, making it more difficult to remove.
Development includes immersing the substrate in a solution that dissolves exposed areas (for positive) or unexposed parts (for negative). The complete procedure is visible in Figure 1.3.

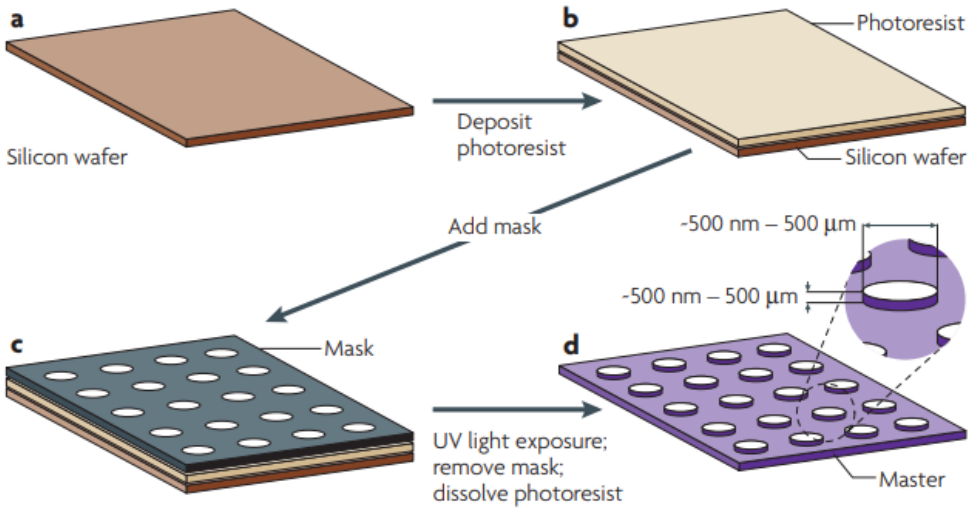

Figure 1.3 *a–b | Photoresist is spincoated on a silicon wafer. c | A mask is placed in contact with the layer of photoresist. d | The photoresist is illuminated with ultraviolet (UV) light through the mask. An organic solvent dissolves and removes photoresist that is not crosslinked. The master consists of a silicon wafer with features of photoresist in bas-relief. An expanded view of one of the microfabricated structures with its characteristic critical dimensions is shown. Adapted from*[12].

Soft lithography can be viewed as a complementary extension of photolithography, but unlike it, soft lithography can process a wide range of elastomeric materials, i.e. mechanically soft materials, most notably PDMS; this is why the term "soft" is used[13].

The basic process consists of building elastomeric microchannels, while the rest of the process depends on which subcategory we are considering; in fact, there are 4 different main subcategories, which are Replica molding (the technique we used in the presented studies), Microcontact printing, Capillary molding and Microtransfer molding[14].

Replica molding involves generating a soft elastomeric copy of a rigid mold (ie. obtained through photolithography). Briefly, the polymer, typically PDMS, is poured into the mold, and allowed to completely polymerize. The replica can then be separated from the mold, which can be reused multiple times, and further processed for the subsequent experimentation[13].

1.1.2.3 Plasma treatment

Once the fabrication is completed, the PDMS platform must be sealed to a glass slide obtaining a perfect hydraulic seal. One possibility, and the most convenient, is plasma treatment.

Plasma, the fourth state of matter, consists of partially ionized gas with electrons, ions, and neutral atoms or molecules. It is generated at atmospheric or low pressure in a vacuum

chamber, utilizing an electric field. By selecting the appropriate configuration and operating conditions, plasma can be applied for cleaning, activation, etching, or coating surfaces[15].
The process, illustrated in Figure 1.4, activates PDMS and glass with plasma, forming electron-free silicon atoms and silanol groups (Si-O-H) on the surfaces, introducing hydrophilic characteristics. Subsequently, the polymer and glass, when brought into contact, establish covalent Si-O-Si bonds.

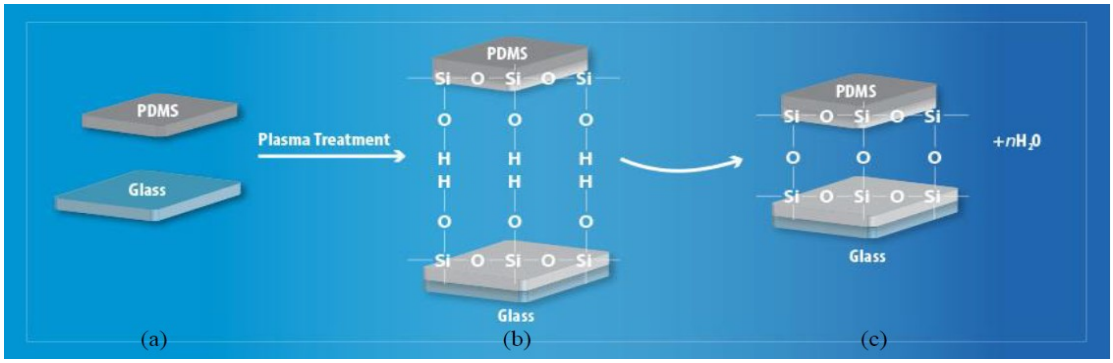

Figure 1.4 *Plasma treatment: (a) single elements of PDMS and glass; (b) activation of the surface; (c) bond creation. Adapted from*[14].

For biological applications, plasma treatment must be performed prior to seeding the cells into the platforms to prevent cellular damage. Plasma treatment shows several advantages: it affects only surface properties, without altering the bulk material; it forms at near-ambient temperature, minimizing the risk of damage to material sensitive to heat; and it can be applied to a wide range of materials.

1.2 Microfluidics in biology

We highlighted so far how the integration of microfluidics and biology could be a key tool in our better understating of cancer, as well as in the toxicology field, offering exceptional contributions to research. Microfluidic platforms, designed to manipulate tiny fluid volumes, more reliably allow to recreate and analyze complex biological processes, especially those related to cancer development and progression[16]. These micro-scale systems enable to better mimic the tumor microenvironment and test the efficacy of drugs and/or xenobiotics with improved precision[16].
This section will provide a comprehensive overview of the tumor types from which we obtained the cell lines employed in our research.

1.2.1 Neuroblastoma

Neuroblastoma (NB) is a rare embryonal solid tumor of the autonomic nervous system and represents one of the most common pediatric diseases[17]. The embryonal origin suggests that NB arises from immature nerve-forming cells known as neuroblasts present in the neural crest tissues. These neuroblasts are then spread throughout the human body. As a result, extracranial tumors can develop in various regions, primarily at the sympathetic system level, which governs vital functions such as breathing and digestion.

Regions commonly affected include the neck, upper chest, abdomen, and pelvis[18]. Some typical pathologies triggered by NB, such as Horner's syndrome and paralysis due to spinal cord compression, are illustrated in Figure 1.5.

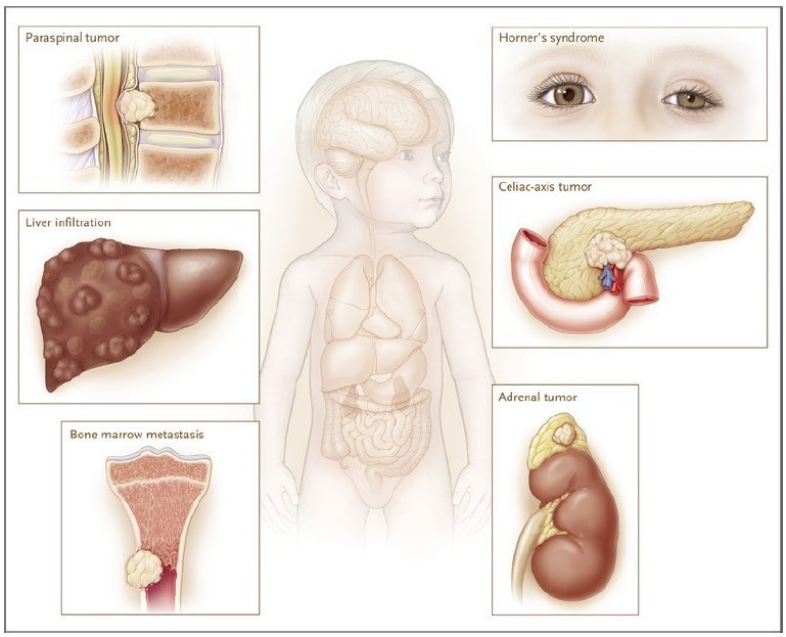

Figure 1.5 *Clinical presentation of NB. Adapted from*[18].

However, the aggressiveness of NB is mainly attributed to its metastatic capability. Tumors diagnosed after the first year of life pose challenges not only in localized areas but also in the abdomen, respiratory system, lymph nodes, and bone marrow. NB cells exhibit the ability to infiltrate organs, surround nerves, and encircle vessels, including the celiac axis, rendering their masses difficult to remove.

1.2.2 Colorectal cancer

Colorectal cancer (CRC) is a major public health problem, being the third most diagnosed cancer and the fourth cause of cancer death worldwide[19].

CRC usually originates from epithelial cells following well-defined pathogenic events; it occurs due to mutations that target oncogenes, tumor suppressor genes and genes linked to DNA repair mechanisms[20].
Generally, the diagnosis of this cancer occurs late, although it is fundamental because of the rapid formation of metastasis, and the high rate of transfer through the bloodstream is one of the primary obstacles in achieving a more effective treatment. Among the risk factors there are: personal and family history, the environment and dietary habits[21].
However, despite a common genetic background, CRC could undergo modifications and proceed along heterogeneous fate in terms of growth, aggressiveness and outcome.

1.3 Comparison of different culture models

In this section, we will survey and compare various culture models, like conventional monolayer cells and three-dimensional spheroids, aiming to show their strengths and weaknesses. By figuring out how well each model works, we hope to improve our toxicological assessments, ensuring better strategies for risk evaluation and overall improvement of human health. Additionally, integrating these models into cancer studies enhances our overall understanding of carcinogenesis and treatment and thus contributes to advancing precision medicine.

1.3.1 Cell cultures

Since the early 1900s, *in vitro* cell cultures have been employed to advance our comprehension of the biological mechanisms governing cellular behavior *in vivo*. Over the course of a century, two-dimensional (2D) cell cultures have served as *in vitro* models to investigate cellular responses to biochemical and biophysical stimuli.
Conventional 2D cultures use adherent, flat surfaces to provide mechanical support to cells growth. In this model, all cells have access to a similar amount of nutrients present in the culture medium and can eliminate metabolites and waste molecules homogeneously, resulting in uniform growth and proliferation[22]. However, this culture system does not provide a tight control on some important cell features, essential for determining cell fate and bioactivity *in vivo*. Additionally, the 2D cell model is too simple and inaccurate in representing the various interactions between cells and their environment, such as cell-to-cell and cell-to-matrix interactions, and tissue organization. Due to their limitations in describing complex biological processes, 2D-based culture systems need to be complemented with further experiments using animal models. However, animal experiments are costly, require large amount of testing materials, and there are large divergences between the animal model and humans, so a complete translation of the results is difficult[23]. Moreover, ethical apprehensions regarding

scientific experiments utilizing animal models have prompted certain organizations to regulate their usage. The European Parliament, through Directive 2010/63/EU, has enacted legislation to safeguard animals employed for scientific purposes, centring the topic on the "3Rs" principle - replacement, reduction, and refinement[24].

In this context, new cellular models have been developed over the years to fill the gap between 2D cell cultures and *in vivo* testing: the three-dimensional (3D) cell culture. In the last years, researchers have increasingly implemented 3D structure-based culture systems, which better mimic the physiological environment biochemically and biomechanically. Cells bioactivity depends on their stimulation from physiological microenvironment, including cell-cell and cell-matrix interactions. In a 3D complex structure, cell clusters grown can imitate *in vivo* cell functions, creating mechanical and chemical gradients.

3D cell cultures are considered more representative models for performing *in vitro* toxicological studies thank to their multiple characteristics of *in vivo* systems, such as the presence of the extracellular matrix (ECM) and a spatial realistic conformation, which translates into a more physiological and accurate biochemical response, compared to 2D cell culture models.

Several 3D cell models have been developed to emulate the natural tissue conformation, enhancing the predictability of laboratory procedures. In general, 3D models can be categorized into three groups: spheroids, organoids, and organs-on-a-chip (Figure 1.6).

Spheroids are used in this work of thesis and will be described in the next section.

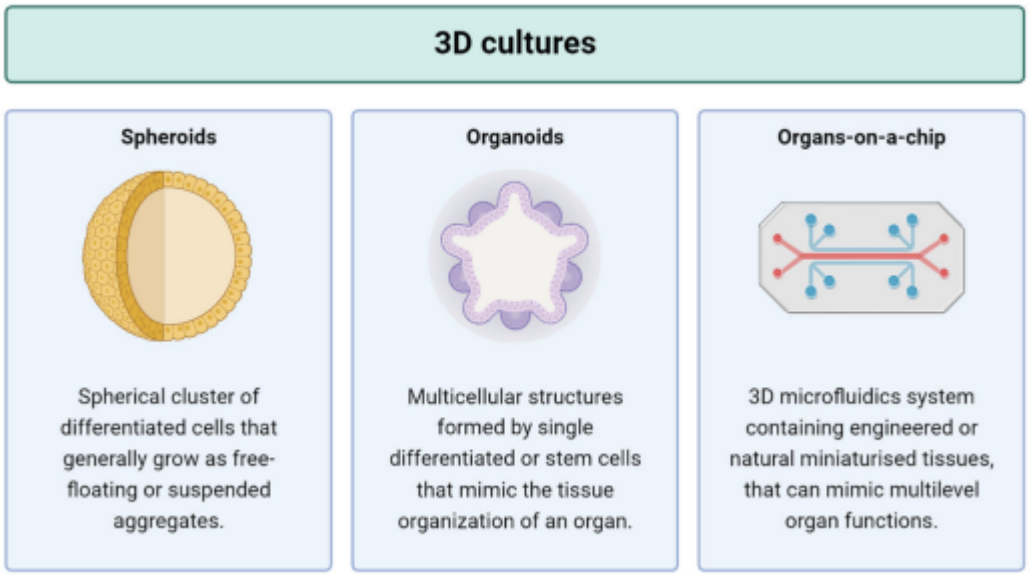

Figure 1.6 *Types of 3D culture systems. Adapted from*[25].

1.3.2 Spheroid models

Spheroids are rounded, low-complexity cell aggregates, typically derived from differentiated cells. Cells come together in loose groups by connecting with specific parts of the surrounding environment. This happens as certain proteins increase on the cell surface. These proteins are called junctions. They facilitate the binding of cells, resulting in the formation of a tightly-knit cellular cluster known as a spheroid. The ideal size for spheroids to replicate *in vivo*-like interactions between cells and establish a gradient of oxygen and essential nutrients is around 500 μm[25]. This is crucial for ensuring the biological relevance in studies in which a tumor model is to be replicated and thus an oxygen and nutrient gradient and the formation of an internal hypoxic portion (core) is required. In this structured arrangement, distinct concentric rings of diverse cell populations can be identified. Moving from the center outward, an inner hypoxic core forms, characterized by necrotic and apoptotic cells due to limited access to nutrients and oxygen. Surrounding the spheroid core is a middle layer of quiescent viable cells, and the outer layer consists of highly proliferative and migratory cells[25].

To obtain reproducible spheroids, various techniques have been developed. The spheroid formation methods are generally classified into two main groups: scaffold-based and scaffold-free methods[26]. Scaffold-based methods use external cell anchoring scaffolds made of natural or synthetic polymers, imitating the natural ECM to support cell growth. Examples include spinner flask[27] and microcarrier beads[28]. In scaffold-free spheroid formation methods, there is no external supporting scaffold, relying on the self-aggregation of cells. Common scaffold-free methods include the hanging drop method[29], magnetic levitation method[30], liquid overlay technique[31], and seeding technique using ultra-low attachment (ULA) plates[32].

3D spheroids can be employed for advanced functional assays to comprehend the biological mechanisms activated by cells. In toxicological studies, viability and cytotoxic assays are frequently used to assess the effects of several compounds. The real limit is the data reproducibility, as the absence of a clear standardized spheroid formation protocol. To reduce variability and increase reproducibility, it is important to optimize the spheroid generation protocol, as well as the protocols for studying functional end-points. Overall, optimization of other established 2D techniques, as staining and imaging, is necessary because of not all substances used in these protocols are able to diffuse into the inner core of the spheroids[33].

1.3.3 Analysis of diverse culture models in the context of mycotoxin cytotoxicity evaluation

Studying the harmful effects of mycotoxins requires looking at different cell models. These natural toxins, produced by filamentous fungi, can be harmful to health, so it is important to assess their toxicity accurately. By using various biological methods like cell-based assays,

researchers can gain different insights into how mycotoxins affect cells and refine their risk assessment. This section will briefly describe the mycotoxins used in this study.

1.3.3.1 Mycotoxins

1.3.3.1.1 General information

Mycotoxins are low-molecular-weight secondary metabolites produced by filamentous fungi. The definition of mycotoxin considers the target and the concentration of the metabolite, in fact not all toxic compounds produced by fungi are classified as mycotoxins. From this point of view, substances made by fungi that fight bacteria are called antibiotics. Fungal products that harm plants are known as phytotoxins, and fungi metabolites that are toxic to animals, especially at low concentrations, are called mycotoxins[34].
Environmental, storage, and ecological conditions are the primary factors contributing to the presence and production of mycotoxins in foods or feeds[35]. Mycotoxins can enter the food chain both by direct contamination of food commodities of plant origin or indirectly by the contamination of food products derived from animals fed with mycotoxins contaminated feed. Humans can be exposed to mycotoxins through diet or by breathing in dust and toxins in the air[36]. Short term exposure to mycotoxins is usually not harmful. However, continuous exposure to these toxins can result in damaging effects like mutations, birth defects, and cancer in both humans and animals.
According to the Rapid Alert System for Food and Feed (RASFF) annual report for 2022, mycotoxins are the third most notified hazard category, with 485 notifications and a 10.5% increase compared to the previous year[37]. This highlights the key role mycotoxins play in food and feed border rejections and economic losses in food industries. Furthermore, their high prevalence explains the ongoing pressure of the scientific community on the importance of continuous monitoring and characterization of the human hazard to ensure food safety[38].
It is important to note that prevention of mycotoxin's formation is partially possible with good processing practice both during pre-harvest and post-harvest stages of food chain. For example, the appropriate use of fertilizers, the removal of residues or debris from previous harvest, timely harvesting, avoiding plant mechanical damage are preventing fungal growth[35].

1.3.3.1.2 Ochratoxin A

Ochratoxin A (OTA) is a mycotoxin of *Aspergillus ochraceus*, but others *Aspergillus spp*. can produce this metabolite.
The structure of OTA consists of a para-chlorophenolic group containing a dihydroisocoumarin moiety that is amide-linked to L-phenylalanine (Figure 1.7).

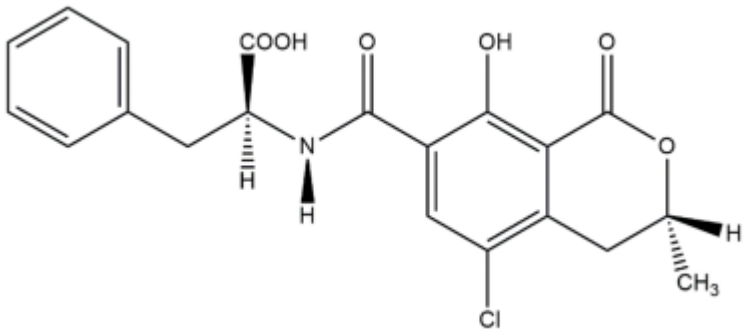

Figure 1.7 *Chemical structure of OTA mycotoxin. Adapted from*[39].

OTA is soluble in water and organic solvents, including methanol[39].
Its production is linked to fungal development, which is influenced by light exposure. Nevertheless, it has been discovered that various factors, such as UV light, oxidative stress, pH, and nutrient sources, can impact the biosynthesis of OTA.
OTA was found in food and feedstuff of both plant and animal origin: cereals, beer, coffee and cocoa products, spices as well as pork and chicken meat products[40].
Some research shows that OTA is nephrotoxic, hepatotoxic, embryotoxic, teratogenic, neurotoxic, immunotoxic genotoxic, and carcinogenic in many species and the toxicity level is sex-related. Overall, OTA has been recognised as possibly carcinogenic to humans and it is classified as an agent belonging to the Group 2B by the International Agency for Research on Cancer (IARC)[41].

1.3.3.1.3 Patulin

Patulin (PAT) was first isolated from *Penicillium griseofulvum*[42], and it became almost immediately evident that PAT was toxic to both plants and animals and classified as mycotoxin. Like other mycotoxins, the production of PAT depends on various factors, including temperature, pH, and other climate and physiological conditions. However, it is not entirely clear what are the optimal conditions for PAT production[43].
In terms of physio-chemical characteristics, PAT is a polyketide lactone (Figure 1.8).

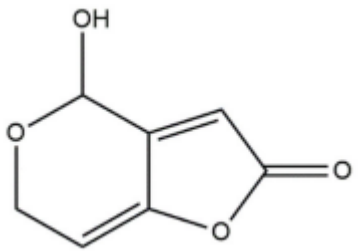

Figure 1.8 *Chemical structure of PAT mycotoxin. Adapted from*[42].

This compound is a heat-stable molecule that cannot be denatured, and it is difficult to metabolize by animals. It is soluble in methanol[44].
PAT has been identified in a variety of food products, mainly fruits and vegetables[45].
Both acute and chronic exposure to PAT can pose risks. Acute exposure may lead to symptoms like nausea, vomiting, gastrointestinal issues, hemorrhages, and intestinal lesions. PAT can also affect the intestinal barrier function[45]. Chronic exposure to PAT may bring about changes in the normal composition of intestinal flora. Additionally, PAT has been shown to have mutagenic, neurotoxic, immunotoxic, and genotoxic effects. PAT has been classified as a group 3 carcinogen (not classifiable as to its carcinogenicity to humans) by the International Agency for Research on Cancer (IARC)[41].

1.3.4 Analysis of diverse culture models in the context of drug testing studies

Similar to the study of mycotoxins, where various cell models are used to study their behavior, examining different models is essential for accurately understanding the effect of drugs, and assessing their effectiveness and potential side effects[46]. Drug testing involves administering medications to target sites within the body, ensuring optimal therapeutic effects[47]. While the previous paragraph focused on mycotoxin toxicity, the following section will briefly describe the specific drug under investigation in this study.

1.3.4.1 5-Fluorouracil (5FU)

5-fluorouracil (5FU) is a chemotherapeutical agent widely used to treat cancers, like breast and colorectal cancers. It works as an antimetabolite to prevent cell proliferation, blocking the thymidine formation required for DNA synthesis[48].
5FU is a heterocyclic aromatic organic compound (Figure 1.9).

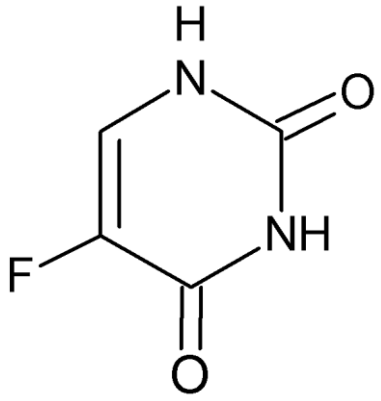

Figure 1.9 *Chemical structure of 5-Fluoroacil (5FU). Adapted from*[48].

Reports of much longer lasting symptoms have been associated with chemotherapy involving 5FU. The more common includes brain fog, confusion and memory impairments which have a significant impact on quality of life and ability to return to work[48].

1.4 Aim of the study

This project aims to develop and validate two microfluidic devices designed to perform specific tasks. The first, will investigate cytotoxicity induced by mycotoxins, the second will generate concentration gradients of selected drugs.

Incorporating advanced design and fabrication methodologies, as well as culture strategies specifically adapted to biological purposes, we aim at addressing poorly understood biological questions.

The first platform, defined SheroFlow Device (SFD), comprises a 3-well chip and houses human NB SH-SY5Y cell spheroids. With its linear design, this device proves to be an innovative tool for easily and precisely assessing cytotoxicity from exposure to mycotoxins, under dynamic conditions.

The second platform, defined MicroGradient Generator (MGG), is designed to generate a gradient of five different drug concentrations, enabling the exposure of human colorectal HCT-15 cell spheroids. This device provides a valuable opportunity to evaluate cytotoxic effects induced by a drug gradient generated directly on the chip.

Through the integration of these two innovative technologies, we expect to significantly increase experimental efficiency, robustness, and reproducibility of results. Our goal is to contribute to the advancement of research in microfluidics, offering state-of-the-art tools for studying cytotoxicity and drug action mechanisms.

Chapter 2

Materials and methods

This second chapter presents the main procedures and protocols optimized during the project. The chapter begins describing the biological protocols for cell maintenance and spheroids production and characterization. It progresses with the design of the platforms and methods for producing the masters and the final devices. Then, the procedures for validating the platforms, with a particular emphasis on fluid dynamics and biological validation are described. In the end, experiments targeted at evaluating the effects of mycotoxins and drugs within the dedicated microfluidic devices are described.

2.1 Biological protocols

This section explains in detail the biological protocols related to cell maintenance, spheroids formation and characterization and GelMA production.

2.1.1 Cell lines

NB cell line (SH-SY5Y; ATCC CRL-2266) is used to evaluate mycotoxins' cytotoxicity, while CRC cell line (HCT15; ATCC CCL-225) is used to evaluate drug cytotoxicity in the gradient chip.

The SH-SY5Y cell line is a thrice cloned subline of the NB cell line SK-N-SH, which was established in 1970 from a metastatic bone tumor from a 4-year-old cancer patient[49].

HCT15 cell line was isolated from the large intestine of a male Dukes C colorectal cancer patient. HCT-15 cells are used in a variety of biomedical studies involving colon cancer proliferation and corresponding inhibitors[50].

2.1.2 Cell maintenance, splitting and counting

Cells are generally seeded in flasks (Corning™) of either 75 cm^2 or 150 cm^2 and kept in an incubator under standard culture conditions at 37°C, in a humidified atmosphere of 5% CO_2, 20% O_2 and pH 7.4. Each cell line grows in a specific culture medium that provides nutrients for their growth.

SH-SY5Y and HCT-15 cell lines are cultured in Dulbecco's Modified Eagle Medium high glucose with L-glutamine (DMEM, ATCC® 30-2002) supplemented with 10% Foetal Bovine

Serum (FBS, ATCC®, 30-2002), 1% penicillin/streptomycin 100X (Corning®, 30-002-CI) and 1% Minimum Essential Medium, Non-Essential Amino Acids (MEM NEAA, Gibco®, 11140-035).
The medium is changed every 3-4 days and cells are passaged once or twice a week using trypsin/EDTA (Corning®, 25-053-CI) for the subculturing procedure.
To maintain optimal cell growth, once the flask reaches a confluence of about 70-80%, cells must undergo subculturing through a splitting procedure. This involves the periodic separation of the cell population, preventing growth arrest and ensuring survival. The extent of subculturing is often denoted as the "passage number," indicating the number of times cells have been transferred from flask to flask.
Both cell lines undergo the same splitting procedure outlined as below.
The cell splitting procedure is conducted under a biosafety cabinet, maintaining sterility. Prior to start, both the culture medium and Trypsin/EDTA (Sigma-Aldrich®) solution are warmed to 37 °C. Next, the protocol can begin:

- Remove the medium from the old flask with a 10 mL serological pipet and store it in a 15 mL Falcon tube;
- Rinse gently the flask with approximately 7 mL of PBS (Gibco™) to remove any trace of culture media that contain Trypsin inhibitors. Then PBS is aspirated and discarded;
- Add 3 mL of Trypsin, an enzyme capable to detach cells from the flask surface, verifying that all the flask bottom surface is covered by the solution, and place the flask at 37°C in a CO_2 incubator for approximately 3 minutes;
- Verify the detachment of the cells under the microscope;
- Add 7 mL of medium inside the flask to inhibit the action of the Trypsin. The solution of cells is pipetted until the achievement of homogeneous cell suspension and placed in a 15 mL Falcon tube;
- Count cells using the Bürker Chamber;
- Centrifuge the cell suspension with soft deceleration to induce the sedimentation of cells at 1200 rpm for 5 minutes;
- Once the centrifugation is ended, the supernatant is discarded, while the pellet of cells is resuspended in a small amount of fresh medium;
- Prepare the new flask by adding 10 mL of medium and an aliquot of the resuspended cells;
- Incubate the flask at 37°C and 5% CO_2.

The quantities of reagents reported are related to the splitting of a 75 cm^2 flask.
To count cells and calculate cellular concentration the Bürker chamber is used. As represented in Figure 2.1, it is formed by a rectangular slide with a chamber engraved with a laser-etched grid, and a 9x9 mm^2 coverslip. The grid has nine squares, each delimitated by three parallel

lines. When the slide and the coverslip are assembled, a chamber of 1/10 mm^3 is created, and cell counting is executed for each of the 9 squares. Specifically, the protocol is:

- Mix 10 µL of Trypan Blue (Invitrogen™), a cell stain that colors dead cells in dark blue, with 10 µL of the cell suspension to be counted;
- Insert 10 µL of the mixture inside the chamber by capillary force;
- Count the number of live cells (bright dots) in each square, observing the chamber at the microscope with a 10x enlargement;
- Calculate the arithmetic mean of cells per square.

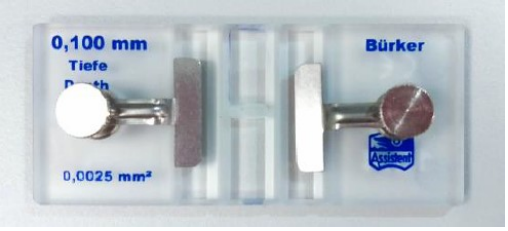

Figure 2.1 *Bürker chamber.*

Finally, cell concentration can be computed using Equation 2.1:

$$N_{cell} = N_{average} \cdot d_1 \cdot V_f \cdot K \tag{2.1}$$

where d_1 is the dilution factor of the cells equal to 2, V_f is the volume of medium in which the cells are suspended, and K is the Bürker Chamber constant, equal to 10000, related to its geometry and volume (number of squares per mL).

2.1.3 Freezing and thawing

Freezing and thawing cell lines is a critical aspect of cell culture maintenance, ensuring long-term viability and experimental reproducibility. Proper cryopreservation protects cells from damage, preserving their genetic integrity and functional characteristics.
The quantities of reagents reported are related to the splitting of a 75 cm^2 flask.
To initiate the freezing process, adhere to the following protocol:

- Remove medium from flask, wash and trypsinize cells. Once cells are detached, add back 5-10 mL media and transfer to centrifuge tube (15mL sterile centrifuge tube);

- Count cells using trypan blue for a viable cell count. The viability should be over 90% to ensure the cells are healthy enough for freezing;
- Cells are centrifuged at 1200 rpm for 5 minutes;
- Resuspend cells in enough freezing medium to create a cell suspension of between $4x10^5$ to $2x10^6$ cells in each freezing vial, depending on the cell line. HCT15 should be frozen in 70% FBS, 20% DMSO and 10% DMEM while SH-SY5Y in 95% DMEM and 5% DMSO. This step must be done quickly as DMSO and some other cryoprotectants are toxic to cells and so should not be exposed to the cells at room temperature for any longer than necessary;
- Transfer cells immediately to -20°C for one hour, followed by -80°C overnight before permanent storage in liquid nitrogen.

Thawing is carried out using the following protocol:

- Prepare pre-warmed medium in advance;
- Remove cryovials from liquid nitrogen and immediately place in 37°C water bath and quickly shake until about 80% has thawed. This should not take more than a minute;
- Cells are then transferred from the cryovial to a 15-mL falcon tube filled with 9 mL of culture media. Subsequently they are centrifuged at 1200 rpm for 5 minutes;
- Remove the supernatant and resuspend the cells in new medium according to the amount of seeding;
- Quickly pipette out into an appropriate flask depending on the cell density, add the appropriate amount of medium and place in incubator. Thawing of the vials and placing of the cell suspension back into culture media should also be done very quickly;
- After 24 hours, ensure cells are attached. Change culture media to remove non-adherent cells and replenish nutrients. Changing the culture media will also remove any DMSO residues.

2.1.4 Spheroid formation and characterization

The spheroid formation protocol is valid for both SH-SY5Y and HCT-15 cell lines.
3D spheroids are generated from single-cell suspensions obtained from trypsinized monolayers cells and diluted to the optimum cell plating density ($2x10^3$ cells/spheroid).
For a 96 well ULA plate (considering 100 wells and 200 µl of medium per well):

- Resuspend the volume of cells corresponding to $2x10^5$ ($2x10^3$/well x 100 wells) in 20 mL of medium (200 µl of medium/well x 100 wells);
- Dispense 200 µL of cell suspension in each well of the plate (you can use the multichannel pipette);
- Centrifuge the plate at 1200 rpm x 5 min.

Once formed, the spheroids are allowed to aggregate and grow for 7 days before being used for experiments.

The software AnaSP® is used to monitor growth and morphological parameters of spheroids[51]. This software analyzes images of spheroids captured under optical microscope, creating a mask for each one. We focused on three specific parameters: solidity, which measures their density, compactness, which assesses their spatial arrangement, and sphericity index (obtained as the square root of circularity), which gauges their sphere-like shape.

2.2 Microfluidic platforms

In this section, materials and methods used to produce the microfluidic devices are described. Starting from the design of the platforms, moving through the production of the master molds, and finally the production of the final devices.

2.2.1 Design of the platforms

2.2.1.1 Design of the Spheroflow Device (SFD)

The first microfluidic platform is based on an existing design. The 2D CAD design of the master is shown in Figure 2.2.

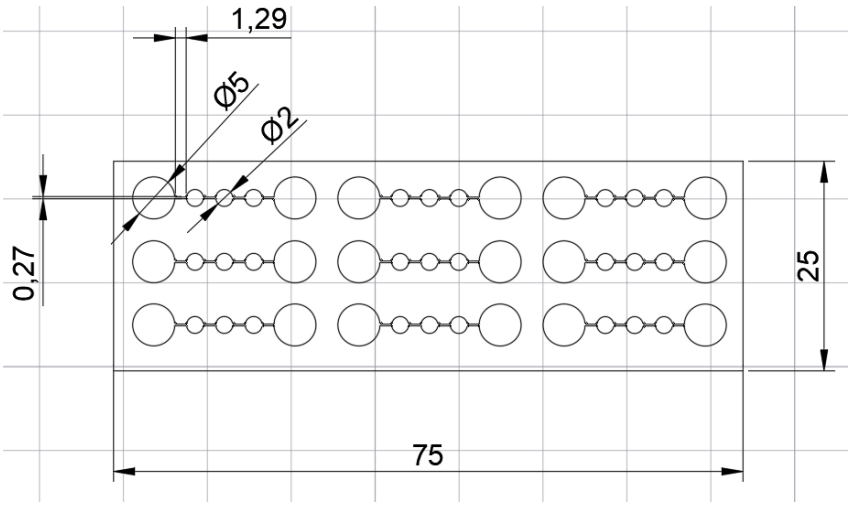

Figure 2.2 *2DCAD design of the first microfluidic platform. Dimensions of the device are given in [mm].*

The platform is composed of nine independent rows of wells grouped into three quadrants. Each row is equipped with an inlet and an outlet reservoir, connected to three wells via microchannels.
This design previously served as a static 2D culture platform, where cells were seeded through the inlet, flowed through channels into the three wells, and adhered, forming a single layer.
For this project, each set of three wells is used individually, with each well accommodating one spheroid.
In summary, each chip features:

- Inlet and outlet reservoirs with a diameter of 5 mm;
- Three wells with a diameter of 2 mm each;
- Microchannels with a length of 1.29 mm and a width of 0.27 mm.

Each chip occupies an area of approximately 25x8.3 mm. The height is 250 μm.

2.2.1.2 Design of the Microgradient Generator (MGG) platform

The optimized geometry involves creating different concentrations of a substance within the same device when connected to a syringe pump. The capability of employing concentration gradient generators in microfluidic systems can be utilized for the rapid screening and exploration of mechanisms that form the basis for the impact of pharmaceutical or chemical compounds on various disease models.
The 2-layers geometry of the device is designed with 3D-CAD software (Figure 2.3) and the master is obtained through soft lithography, with the technique already explained in paragraph §1.1.2.2. In the upper layer, the channels are 0,5 mm wide, and the chambers have a diameter of 2,5 mm. In the bottom layer, the chambers are 12 mm length and 2 mm wide. Porous polycarbonate membranes separate the two layers, so that the flow does not disturb the spheroids. The top inlets are connected to the syringe pump, allowing the formation of different concentrations of the injected substances. The chambers in the lower layer, in contact with those in the upper layer, accommodate cells or spheroids.

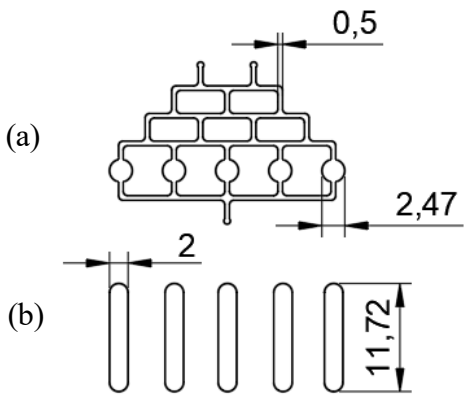

Figure 2.3 *Drug testing chip geometry. Upper layer (a) and bottom layer (b). Dimensions of the device are given in [mm].*

2.2.2 Production of the master

2.2.2.1 Design of the photomask

As explained in §1.1.2.2, the goal is to create a negative photomask that, when placed over the photosensitive resin, allows crosslinking only in the transparent areas after exposure to UV light.

For this purpose, the platform geometry designed in AutoCAD® is imported into Adobe Illustrator® to properly color the different areas of the mask.

Figure 2.4 shows the photomask obtained to produce the chip for mycotoxin cytotoxicity evaluation.

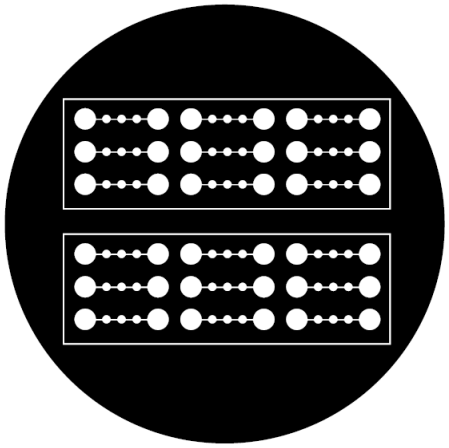

Figure 2.4 *Negative photomask of the mycotoxin cytotoxicity evaluation chip.*

Figure 2.5 shows the photomask including both layers, obtained to produce the dedicated drug testing chip.

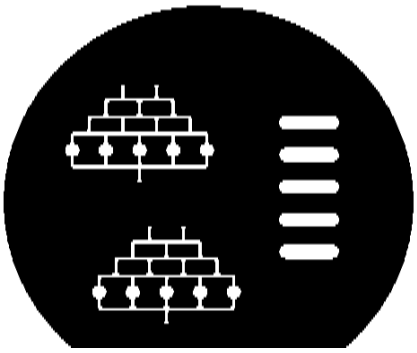

Figure 2.5 *Negative photomask of the drug testing chip.*

The next steps in the production of the master are the same for both devices.

2.2.2.2 Pre-treatment of the silicon wafer

A 10 cm diameter silicon wafer is rinsed with acetone, methanol, and distilled water and dried using a clean stream of compressed air. Subsequently, the silicon wafer is positioned within a desiccator saturated with hexamethyldisilazide vapors (Sigma-Aldrich®) for 15 minutes. This step is crucial to promote the adhesion of the photoresist.

2.2.2.3 Deposition of the initial photoresist layer

After completing the pre-treatment, the wafer is positioned on a spin-coater (SPS Spin 150 wafer spinner) connected to a vacuum pump.
The protocol is valid for both microfluidic devices since they both have the same thickness.
Initially, a layer of 5 μm thick cover using SU-8 2005 photoresist (MicroChem) is made. The silicon wafer previously cleaned is placed and fixed on the spin coater turntable and is covered by the photoresist. To obtain a thickness of 5 μm, the following values for time, velocity and acceleration are set:

- Spin at 500 rpm for 10 seconds with an acceleration of 100 rpm/s;
- Spin at 3000 rpm for 35 seconds with an acceleration of 300 rpm/s.

Following the spin-coating process, the wafer is then carefully transferred to a flat surface and allowed to rest for a duration of 5 minutes.

2.2.2.4 Soft bake and exposure

The wafer undergoes a soft bake (SB) on a hotplate at 95°C for 5 minutes. This process enables to eliminate internal stresses in the material and evaporate any solvent traces present

in the photoresist. Following the soft bake, the wafer is then covered with the photomask and exposed to UV light. Expose the photoresist layer to UV light (105 mJ/cm^2) without photomask for 3 minutes as it is sufficient to create a first layer without a geometric pattern.
The exposure energy (E_{exp}) is determined based on the thickness of the photoresist, and the corresponding exposure time (t_{exp}) is calculated using the lamp power (P), as per Equation 2.2.

$$t_{exp} = \frac{E_{exp}}{P} \tag{2.2}$$

2.2.2.5 Post-exposure bake of the initial photoresist layer

The Post-Exposure Bake (PEB) serves as a heat treatment to ensure the full cross-linking of the photoresist. After exposure, the wafer is placed on hot plate at 95 °C for 3 min so that total cross-linking of this first layer takes place.

2.2.2.6 Deposition of the main photoresist layer

SU-8 2100 negative photoresist (MicroChem) is poured onto the wafer previously secured to the spin coater. A final thickness of 250 is obtained μm by setting the following parameters:

- Spin at 500 rpm for 10 seconds with an acceleration of 100 rpm/s;
- Spin at 1000 rpm for 32 seconds with an acceleration of 300 rpm/s.

Once removed from the spin coater, the wafer is placed on a flat surface for at least 10 minutes.

2.2.2.7 Soft bake and exposure of the main photoresist layer

As in step §2.2.2.5, the wafer is placed on a hot plate at 95 °C for 45 minutes. Then, the photomask is placed on the wafer, which is exposed to UV light with a power of 350 mJ/cm^2 for 120 seconds toobtain the selective crosslinking of the parts of layer corresponding to the transparent areas of the photomask, through which UV rays pass through.The power and exposure time depend on the thickness of the photoresist deposited on the wafer (250 μm), as per Equation 2.2.

2.2.2.8 Post-exposure bake of the main photoresist layer

A second cross-linking is performed on a hot plate at 95 °C for 15 minutes.

2.2.2.9 Development

The wafer is immersed in a beaker containing propylene glycol monomethyl ether acetate (Sigma-Aldrich®) for 17 minutes. Then, the wafer is placed on the oscillator set at maximum speed. The development process is needed to remove all the excess polymer that has not been cross-linked.

2.2.2.10 Rinsing and drying

After the 17 min has elapsed, the wafer is rinsed again with propylene glycol monomethyl ether acetate (methoxy) and then with isopropanol (IPA, Sigma-Aldrich®). Then, the surface is dried with compressed air.

2.2.2.11 Hard Bake

The final heat treatment, Hard Bake (HB)enhances the mechanical and thermal characteristics of the master. The wafer, shielded with aluminum foil, is positioned on a hot plate at 65°C for 10 minutes; and then from 65°C to 160°C at a rate of 120°C/h for 2 hours.

2.2.3 Manufacturing the platforms

The PDMS platforms are manufactured through replica molding and plasma treatment. As detailed in §1.1.2.2, replica molding is a soft lithographic technique utilizing a master and a polymer to replicate the device, while plasma treatment facilitates the creation of a flawless hydraulic seal between the PDMS microfluidic platform and a glass slide. Prior to replica molding, the surface of the master mold undergoes treatment with chlorotrimethylsilane vapors (Sigma-Aldrich®) for a minimum of 1 hour. This treatment aims to preserve the integrity and definition of the channels and promote the detachment of PDMS from the master.

2.2.3.1 Replica molding

The kit PDMS Sylgard® 184 (Dow Corning) is used for the fabrication of both the platforms. This is a two-part kit containing a silicon elastomer base and a curing agent as depicted in Figure 2.6.

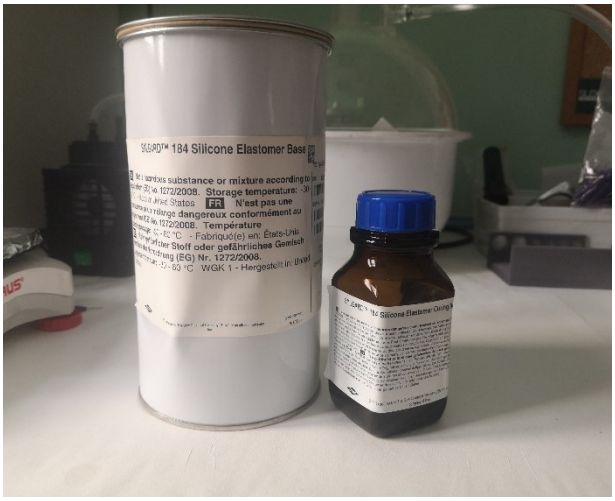

Figure 2.6 *PDMS Sylgard® 184 (Dow Corning), two-part kit: curing agenton the left, silicone elastomer base on the right.*

The steps of the replica molding process are:

- Weight the elastomer and the curing agent in a proportion of 10:1 inside a plastic cup;
- Mix energetically the solution until the formation of a homogeneous solution. During this step, a large number of air bubbles is formed inside the mixture;
- Put the mixture in a desiccator connected to a vacuum pump to remove air bubbles. This step is repeated many times until the solution is clear;
- Pour the PDMS mixture on the master and place it again in the desiccator for additional bubble removal;
- Cure the PDMS on the master inside an oven at 80°C for 45 minutes.

Remove the cured PDMS from the master. Before plasma treatment, the obtained platforms are redefined by cutting off the excess PDMS around the geometry. The inlets and outlets of both chips are punched with 1-mm punch, while 2-mm punch is used for the spheroid housing wells.

In the replica molding process of the chip designed for mycotoxin cytotoxicity evaluation, a supplementary layer of PDMS is applied onto the initial layer The first layer contains the primary geometry, while the second layer is created by punching 2 mm holes in an additional PDMS layer, devoid of any specific geometry. Moreover, the PDMS cylinders with a 2 mm well diameter, produced from the punching of the second layer, serve as plugs to finalize the platform assembly.

2.2.3.2 Plasma treatment

Once the fabrication is complete, a hydraulic seal between the PDMS platforms and the glass slides is obtained through plasma treatment. Furthermore, plasma treatment is utilized to ensure a secure seal at PDMS-PDMS interfaces to produce double-layer microfluidic devices. For the chip dedicated to mycotoxin cytotoxicity evaluation a glass slide of 25x75 mm is used, while for the chip designed for evaluating drug cytotoxicity a76x52 mm glass slide is used.

The main steps, identical for both devices, are:

- Clean the device and the glass slide from any dust residues with scotch tape;
- Insert the three pieces (the two PDMS layers and the glass slide) inside the Plasma Cleaner (PDC-002-CE by Harrick Plasma) chamber shown in Figure 2.7 (a), and close both the door and the valve. The surfaces to be activated must be faced upwards;
- Switch on the vacuum pump to create vacuum inside the chamber;
- After 4 minutes the plasma is turned on and once a dull pink appears, the valve must be regulated to obtain an intense pink color, as represented in Figure 2.7 (b). This correlates with the ideal percentage of oxygen to promote a good surface activation;
- After approximately 1 minute both the plasma and the vacuum pump are switched off and the valve is slowly opened to restore the atmospheric pressure;
- Put the two PDMS pieces in conformal contact and finally attach them over a glass slide, allowing the formation of covalent bonds between all the parts;
- Place the microfluidic platform in an oven for 5 minutes at 80°C to strengthen binding.

Figure 2.7 *Plasma treatment: (a) plasma Cleaner by Harrick Plasma used in BIAMET Laboratory; (b) color of plasma when an adequate quantity of oxygen is present in the chamber.*

2.3 Validation of the Spheroflow device (SFD)

Fluid dynamic and biologic validation of microfluidic devices is crucial for ensuring their functionality and reliability. This process ensures accurate fluid behavior within the devices and validates their compatibility with biological samples. In the following, the fluid dynamic and biological validations of the device that assesses the cytotoxicity of mycotoxins are illustrated.

2.3.1 Fluid dynamic validation

The hydraulic seal validation of the microfluidic platform is performed using coloured tracers diluted in milliQ water. Fluid dynamic validation can be performed either by direct injection of the solutions with a micropipette or by using a syringe pump.

If a syringe pump is used, syringes are filled with colored solutions, fixed to the PHD Ultra pump (Harvard Apparatus), and connected by silicone tubes to the inlet of the microfluidic device. Outlets are connected to 1 mm tips to complete the configuration and collect the outgoing dye. PDMS well-diameter plugs are employed to prevent any dye leakage from the seeding wells. The pump is configured to operate at a flow rate of 1 µl/min, and the chip is continuously perfused for 24 hours. To confirm fluid-dynamic validation, the chip is deemed successful only if the tip inserted into the outlet is entirely filled with dye, and there is no dye leakage observed between the two layers of the chip and around the wells covered by the plugs at the end of the perfusion period.

2.3.2 Biological validation

Biological validation involves optimizing the culture of spheroids inside the chip and evaluating their viability.

To biological validate the chip, the process involves connecting the chip with seeded spheroids to a syringe pump. Subsequently, the viability of the spheroids is evaluated after exposure to constant flux of complete growth medium for 24 hours.

Before initiating the biological validation, the chip and microtubes must undergo autoclaving (Europa B Evo, Arco Scientifica) for sterility assurance. Simultaneously, all required solutions need preparation within a bio-safety cabinet. To eliminate any bubbles from the microchannels of the device, a de-bubbling step is essential. This can be achieved by flowing physiological water into the channels using either a micropipette or an additional syringe.

The optimization of the chip performance also requires the removal of any air bubbles from the syringes and tubes that are connected to the microfluidic platform. Finally, the biological validation itself is conducted by placing 7-days-old SH-SY5Y spheroids (1 spheroid per well) into the seeding wells. Spheroid loading is performed by manually transferring individual

spheroids into the seeding well of the device. Particularly, each spheroid, extracted from the 96-well ULA growth plate using a micropipette with a cut tip, is gently released by gravity into the seeding well. Subsequently, all seeding wells are covered with PDMS well-diameter plugs to seal the system and a flow rate of 1 µl/min of culture medium is applied.

2.3.2.1 Cell viability assay

To assess cell viability inside the microfluidic platform, a cell viability assay is performed on spheroids directly inside the microfluidic chamber. The Live&Dead assay consists in staining cells using fluorescent substances that have specific affinity to one substrate, so that they mark one specific target selectively. The staining solution is prepared diluting three cell markers in 1xPBS:

- Hoechst 33342 (used in a volume ratio 1:500) it is a blue, fluorescent dye which marks all cell nuclei. Its excitation wavelength is equal to 361 nm while the emission one is equal to 461 nm;
- Calcein-AM (used in volume ratio of 1:1000)it is a green, fluorescent dye which marks the cytoplasm of living cells. Its excitation wavelength is equal to 495 nm while the emission one is equal to 515 nm;
- Propidium Iodide (used in volume ratio of 1:400) it is a red fluorescent dye which marks the death cell nuclei. Its excitation wavelength is equal to 535 nm while the emission one is equal to 617 nm.

Firtsly, three 5-minuntes washes with 1xPBS are performed. Next, the staining solution is injected, and the device is placed in the incubator for at least 40 min. Another three 5-minutes washes with 1xPBS are performed. Finally, the spheroids in the platform are visualized using a fluorescence microscope.

2.4 Validation of the Microgradient generator platform (MGG)

Below the fluid dynamic and biological validations of the device for drug testing is described. For the fluid dynamic validation, a software for numerical simulations called COMSOL Multiphysics® is also used, to confirm the establishment of the concentration gradient more precisely.

2.4.1 Fluid dynamic validation

2.4.1.1 Fluid dynamic validation with colorant and fluorescein isothiocyanate labeled dextran

The device underwent validation using colorant and fluorescein isothiocyanate labeled dextran. In both scenarios, the device is linked to a syringe pump, with the left inlet connected to a syringe containing colorant or labeled dextran, and the right inlet to a syringe containing PBS. Also in this case, the pump is configured to operate at a flow rate of 1 µl/min. The validations verified the creation of five distinct concentrations, with a higher concentration in the left chamber gradually diminishing towards the right. Additionally, steady-state conditions were sustained for several hours in these instances.

2.4.1.2 Fluid dynamic validation with COMSOL Multiphysics

The COMSOL Multiphysics® modelling software is used to simulate the fluid dynamics of the microbioreactor, and to understand the shape and relative concentrations of the gradient inside the microfluidic device[52]. The software is organized in modules, each selected to add a specific physics interface to the system. The physics that are added to this simulation are: *a*. the laminar flow of a single-phase incompressible fluid to describe fluid motion inside the channels, and *b*. the transport of a diluted species to simulate the diffusive behavior of a generic species *i* inside the platform. The fluid inside the microbioreactor is assumed to be water, since its physical properties are comparable to the ones of the solutions used during the experiments[52].
A single-phase fluid laminar flow is described by the Navier-Stokes Equation (Equation 1.1), that is solved considering the fluid as Newtonian, its density as constant (temperature is considered as constant). The no-slip boundary condition applies to the walls. The problem is analyzed setting a *time dependent* study to evaluate fluid behavior during a period of time between 0 and 24 hours. The parameters that are specified to solve the laminar flow are:

- A temperature of 37°C;
- An inlet medium velocity between 1 to 10 µL/min for simulating different inlet flow rates;
- An outlet pressure of 0 Pa.

The study of the behavior of chemical species transported by diffusion is fundamental for the objective of the device. The species can be assumed as diluted since their concentration is small if compared to the one of the solvents. Mixture properties such as density and viscosity

are assumed as those of the solvent. Fick's law can be applied to describe the diffusion of the solute, as explained in paragraph §1.1.1.
Coupling this physics interface with the laminar flow, the velocity term can be calculated by keeping the convective term active. The parameters that must be defined are[52]:

- The diffusion coefficient, that is changed to simulate the different types of solute that can be flown through the lateral channels;
- The initial concentration *c* (at the inlets) of the species.

The characteristics of the species, except for the diffusion coefficient, are not needed since the solution is assumed to be extremely diluted. Therefore, the properties of the solute do not affect the solvent's ones and consequently also its behavior.

2.4.2 Biological validation

In this part of the project an hydrogel is used to encapsulate CRC spheroids. The goal of this choice is to create a scaffold for spheroids that could better mimic the physiological environment of cells. The hydrogel used in this case is gelatin methacrylate (GelMA), a widely studied and used hydrogel, also in BIAMET laboratory. GelMA is a gelatin derivative containing a majority of methacrylamide groups and a minority of methacrylate groups that confers to gelatin the property of photocrosslinking with the assistance of a photoinitiator and exposure to UV light. Polymerization can take place at mild conditions (room temperature, neutral pH, in aqueous environments, etc.) and this enables microfabrication of the hydrogels to create unique patterns, morphologies, and 3D structures, providing ideal platforms to control cellular behaviors and to engineer tissues. The photoinitiator chosen for this purpose is lithium phenyl-2,4,6-trimethylbenzoylphosphinate (LAP)[53].
GelMa used in this experiment is concentrated to 8% w/v and is mixed with 0.1% LAP.
The microfluidic platform is placed inside a Petri dish, and HCT-15 spheroids grown for 7 days inside a 96 well ULA plate, are transferred inside an Eppendorf containing 150 µl of previously prepared GelMA. This solution is gently mixed and then 25 µl of the spheroids-GelMA mix is injected into each chamber. Next, GelMA crosslinking is performed with UV light for one minute per well.
First the device is connected to the pump and two 5 mL syringe are filled with 5 mL of the correct medium. Next the two syringes are connected to the two inlets of the microfluidic device paying attention to eliminate all the air bubbles inside the tubes.
Subsequently, a flow rate of 1 µL/min is set, and the pump (PHD Ultra by Harvard Apparatus) infusion is started. Finally, the device is stored in the incubator for 3 days while the pump continuously infuses medium inside the platform.

2.4.2.1 Cell viability assay

To assess cell viability inside the microfluidic platform, a Live&Dead assay is performed on spheroids seeded inside the microfluidic chambers of the multi concentration device. The procedure is similar to the one described in paragraph §2.3.2.1.

2.5 Cytotoxicity of individual mycotoxin exposure on 3D spheroids

The final protocols implemented for the evaluation of mycotoxin cytotoxicity are described below.

2.5.1 Experimental set-up

The protocol is as follows:

- Apply a coating of 1% Pluronic in PBS to the chip's surface for 24 hours;
- Perform debubbling using physiological water;
- Substitute physiological water with complete medium;
- Seed SH-SY5Y spheroids on chip, 1 spheroid per chip well;
- Use tweezers to insert plugs, previously prepared with a 2 mm punch, into the chip, paying attention to the depth of insertion to ensure stability and proper functioning. In this step the chips should be well covered with medium to avoid air bubbles formation during spheroid insertion;
- Fill 5 mL syringe with OTA and PAT at varying concentrations, TritonX, Medium and Methanol (MeOH) in a final volume of 2 mL;
- Place the syringes and their corresponding tubes on the pump in the appropriate slots and secure tightly with screws making sure that the syringes are all equally oriented;
- Start the pump with a flow rate equal to 1µL/min;
- Insert tubes needle into the corresponding chips.

The concentrations of OTA are as follows: 6.25, 12.5, 25, 50, 100 µM in 2 mL of DMEM. Meanwhile, the concentrations of PAT are: 3.12, 4.5, 6.25, 9, 12.5 µM in 2 mL of DMEM.
For each experiment, a negative control (syringes containing only DMEM), a solvent control (syringes containing containing the same amount of MeOH) and a positive control (syringes containing 20 µL/mL 1% TritonX) were included.
At least three replicates are performed for each condition, and those in which the chips are not functioning optimally are discarded. Each chip is housed within a petri dish, facilitating the collection of medium exiting the device's outlet.
At the end of mycotoxin exposure, the chips are detached from the syringe pump, a cell viability assay is performed like in paragraph §2.3.2.1. Spheroids are taken out, and MTT test is performed.

2.5.2 MTT Assay

The MTT assay is a method based on the ability of viable cells to metabolize the yellow soluble tetrazolium salt to a blue insoluble formazan product by the mitochondrial succinic dehydrogenase[54].

The protocol is executed as follows:

- Spheroids are individually transferred to a flat bottom 96-well plate with 100 µL of supernatant and 50 µL/well of MTT solution (5 mg/ml) are added;
- After 4 h of incubation at 37°C protected from light, the resulting formazan crystals are solubilized in DMSO (50 µl/well);
- Finally, the absorbance is measured at 560 nm using Wallace Victor2, model 1420 multilabel counter (PerkinElmer).

2.6 Drug testing on 3D spheroids

The protocol implemented for the evaluation of drug cytotoxicity is described below.

2.6.1 Experimental set-up

The microfluidic device is prepared like in paragraph §2.4.2.

Once the spheroids-GelMA solution is injected inside the chambers and the crosslinking under UV light occurs, the device is connected to the pump:

- Two 5 mL syringe are filled with 3 mL of the correct medium;
- The two syringes are connected to the two inlets of the microfluidic device paying attention to eliminate all the air bubbles inside the tubes;
- A flow rate of 1 µL/min is set, and the pump infusion is started.

The device is stored in the incubator for 24 hours while the pump continuously infuses medium inside the platform.

At this stage, the drug test is conducted, exploiting the device capability to generate 5 different concentrations of a specific substance:

- The left syringe is filled with 3 ml of 5FU, while the right one is filled with 3 ml of culture medium;
- The two syringes are connected to the two inlets of the microfluidic device paying attention to eliminate all the air bubbles inside the tubes;
- A flow rate of 1 µL/min is set, and the pump infusion is started.

The device is stored in the incubator for 72 hours while the pump continuously infuses the drug and the medium inside the platform.

At the end of the experiment, a cell viability assay (§2.3.2.1) is performed to qualitatively evaluate the cytotoxicity of the drug on CRC spheroids.

Chapter 3

Results

3.1 Cytotoxicity of individual mycotoxin exposure on 3D spheroids

This section will discuss the results of the experiment conducted with the chip for cytotoxic evaluation of mycotoxins Patulin and Ochratoxin.

3.1.1 NB spheroid production and characterization

Neuroblastoma spheroids were produced using the cell line SH-SY5Y. SHSY5Y spheroids are generated following the procedures outlined in paragraph §2.1.4. Their growth progression is observed through microscopic analysis, while AnaSP software is employed to assess their morphology at days 2, 4, and 7. In Figure 3.1 (a), the spheroid on day 2 exhibits a translucent appearance, indicative of its recent formation and the early-stage growth of constituent cells. On day 4, the constituent cells within the spheroid demonstrate attachment to one another, initiating the growth process. In Figure 3.1 (b), the spheroid exhibits a darker appearance, indicative of an increased cell density.
By day 7, after internal structural rearrangements, the spheroid appears more compact and well-defined (Figure 3.1 (c)).

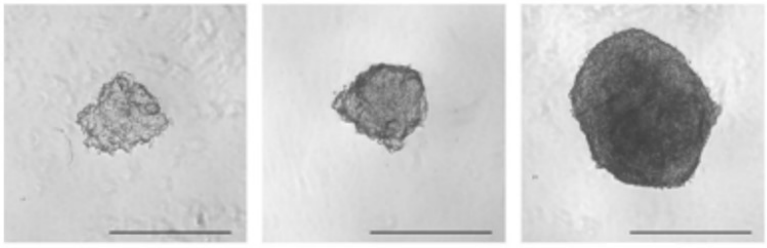

Figure 3.1 *Schematic representation of the process of spheroid's formation:(a) formation of a loose aggregate (b) middle stage of spheroid growth (c) example of spheroid formation derived from SH-SY5Y cells. Scale bar 500 µm; objective 4X.*

Utilizing AnaSP-derived data, a graphical representation depicted in Figure 3.2 is constructed. Notably, on day 2, compactness, sphericity, and SI metrics display higher values compared to day 4. This discrepancy can be attributed to the initial regularity of the spheroid, as the

constituent cells have not yet undergone significant rearrangement or completed growth. Following a reduction in compactness, sphericity, and solidity on day 4, there is a modest increase on day 7, indicating spheroid stabilization and progression towards regularized growth.

These parameters are crucial in the selection of the spheroids to be used for the experiment. Particular focus is dedicated to SI: for values of SI ≥ 0.9 the spheroid is spherical, for values between $0.7 \leq SI < 0.9$ the spheroid is elliptical in shape, and for values of $SI < 0.7$ the spheroid is irregular in shape.

Spheroids meeting the criterion ($SI \geq 0.9$) were achieved by day 7 (Figure 3.2), establishing the timeframe for obtaining experimentally suitable spheroids.

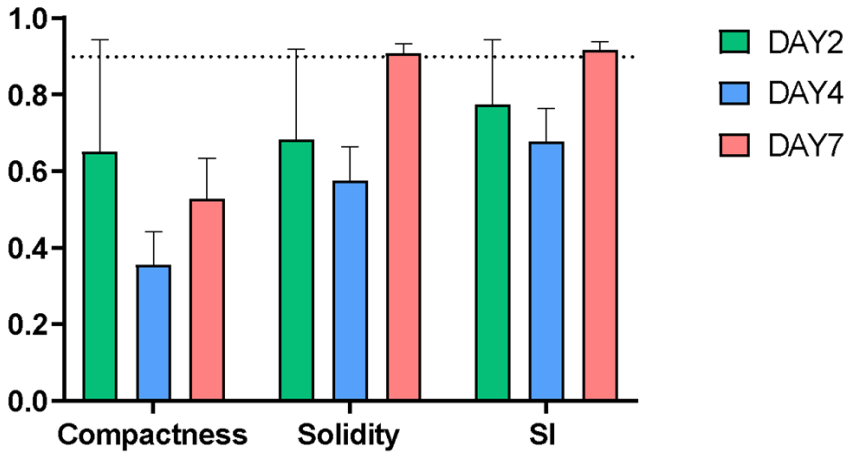

Figure 3.2 *Variation of compactness, sphericity, and SI parameters of spheroids of Sh-SY5Y at days 2,4 and 7. Graph obtained via GraphPad, from data extracted from AnaSP®.*

3.1.2 Platform validation

3.1.2.1 Fluid dynamic validation

Fluid dynamic validation is performed as described in paragraph §2.3.1.
To confirm fluid-dynamic validation, the chip is deemed successful only if the tip inserted into the outlet is entirely filled with dye, and there is no dye leakage observed between the two layers of the chip and around the wells covered by the plugs at the end of the perfusion period.
In Figure 3.3 the correct fluid dynamic validation of the chip can be observed.

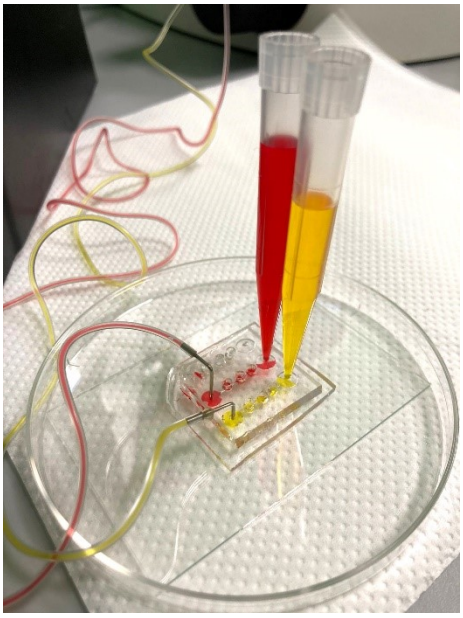

Figure 3.3 *Fluid-dynamic validation of the device. No dye leakage was observed during 24h perfusion with PHD Ultra pump (Harvard Apparatus).*

3.1.2.2 Biological validation

Biological validation is performed as in paragraph §2.3.2. Before settling on the double-layer configuration as the ultimate design, the single-layer configuration is initially explored. However, during biological validation with the pump, the single-layer chip faces challenges. Specifically, the spheroids, once seeded, experienced compression against the well walls, as illustrated in Figure 3.4, preventing successful validation.

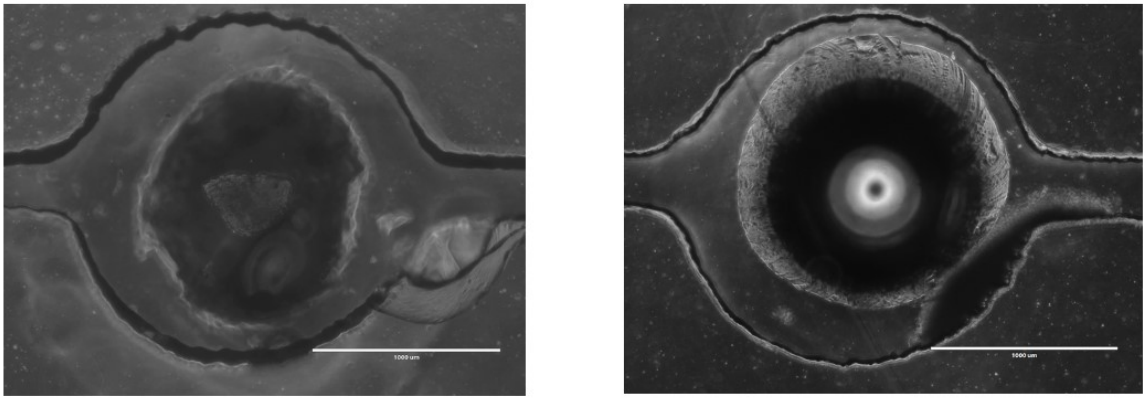

Figure 3.4 *(a) SH-SY5Y spheroid seeded on chip (t = 0) (b) SH-SY5Y spheroid after medium exposure at flow rate of 1µl/min (t = 24). Scale bar 1000 µm.*

The double-layer configuration proved advantageous in this context as it ensured that the seeded spheroids were shielded from direct exposure to the flow, allowing them to maintain their original form. Figure 3.5 illustrates the chip containing spheroids that are initially seeded at the onset of the experiment.

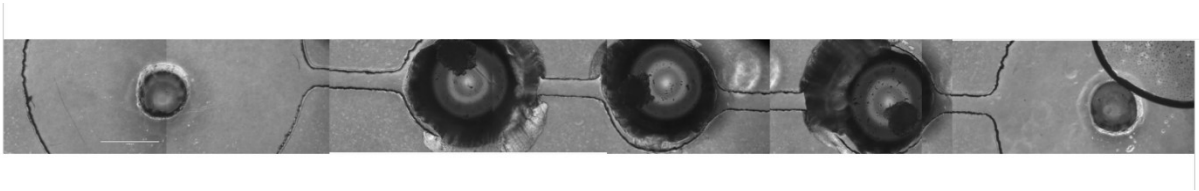

Figure 3.5 *SH-SY5Y spheroids seeded on chip (t = 0).*

In Figure 3.6, a spheroid is depicted after being exposed to the flow for 24 hours. The image clearly shows that the spheroid has retained its original spherical shape, a result attributed to the effectiveness of the double layer in preventing flux-induced deformation.

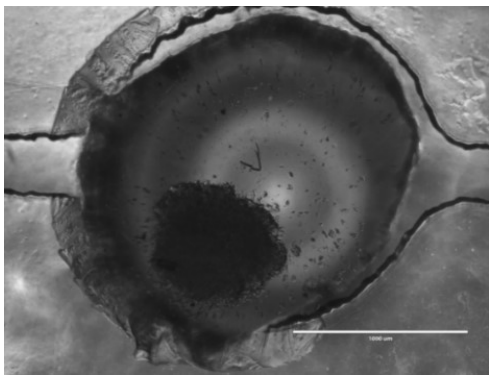

Figure 3.6 *SH-SY5Y spheroid after medium exposure at flow rate of 1µl/min (t = 24). Scale bar 1000 µm.*

Biological validation is further conducted by assessing cell viability, a crucial step to ensure the reliability of the study. It is imperative to confirm that the spheroids, once seeded in the chip, can effectively absorb nutrients from the medium stream, sustaining their vitality without distorting the subsequent assay reading and outcome. The viability of the assay relies on the spheroids' ability to survive exclusively under exposure to the medium within the chip. To address this, a Live&Dead assay is performed, examining the spheroids present in the chip after 24 hours of exposure to the flow. This colorimetric assay utilizes three dyes: Hoechst in blue for the nuclei of all cells, Calcein in green for the cytoplasm of live cells, and Propidium red for the nuclei of dead cells. Figure 3.7 illustrates the results, where the bright green shade attests to the presence of live cells, while the absence of red signals indicates the absence of dead cells. Consequently, the microfluidic platform stands validated from a biological standpoint as well.

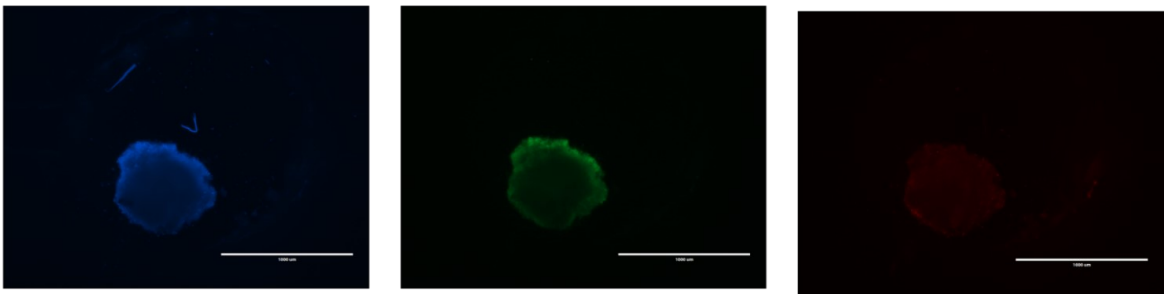

Figure 3.7 *Live and dead assay of SH-SY5Y spheroids after 24h of DMEM exposure in the microfluidic chip at flow rate of 1µl/min. Scale bar 500 µm.*

3.1.3 Mycotoxin cytotoxicity evaluation

3.1.3.1 Live&Dead assay

After 24h of OTA exposure, the Live&Dead assay is performed as described in section §2.3.2.1.
In Figure 3.8, the results from the exposure of NB spheroids to 24h of different concentrations of OTA are respected.

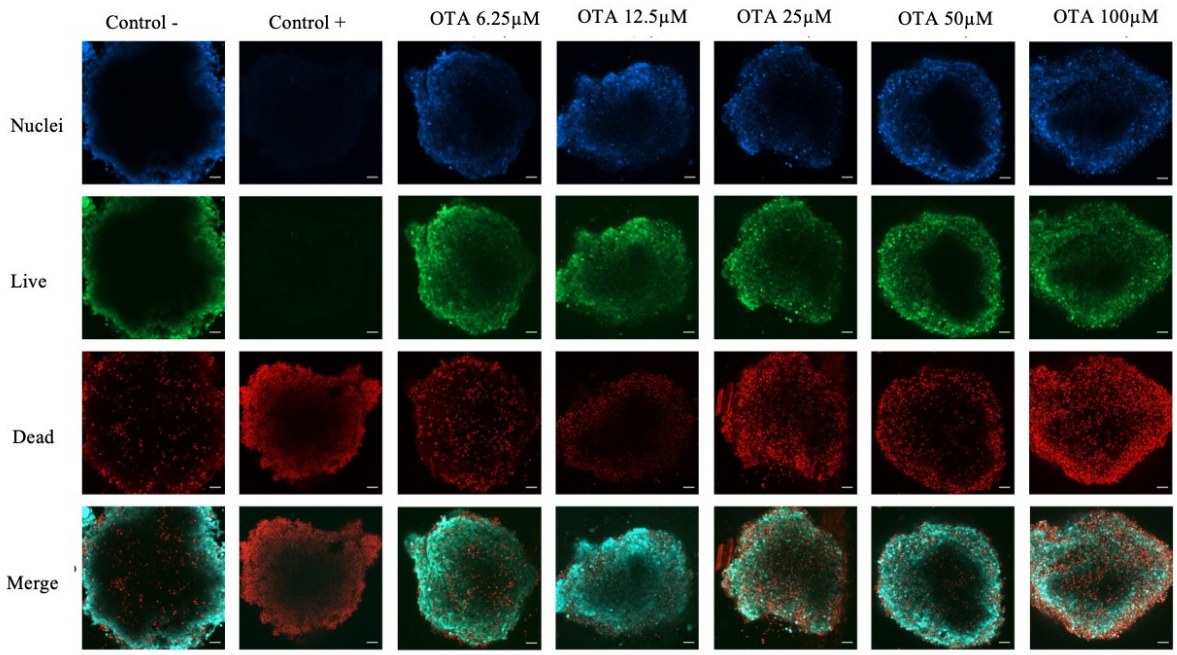

Figure 3.8: *Viability assessment of SH-SY5Y 3D spheroids after 24 hours of exposure to selected concentrations of OTA mycotoxins. Cell's nuclei were staining with Hoechst, live and dead cells were stained using fluorescent calcein-AM and ethidium homodimer-1, respectively. Scale bar 100 µm; objective 10X.*

As depicted in the figure, red colour denotes increasing cellular mortality, peaking at concentration 12.5 µM. Interestingly, concentration 6.25 µM exhibits slightly higher mortality than 12.5 µM. The central region of spheroids remains unstained due to uneven dye penetration within the three-dimensional cellular construct. Live&Dead assessment after 24h affirms cytotoxic effects of a 24-hour OTA exposure on SH-SY5Y spheroids.

Figure 3.9 shows the results about the Live&Dead conducted on SH-SY5Y spheroids after 24h exposition of PAT toxin.

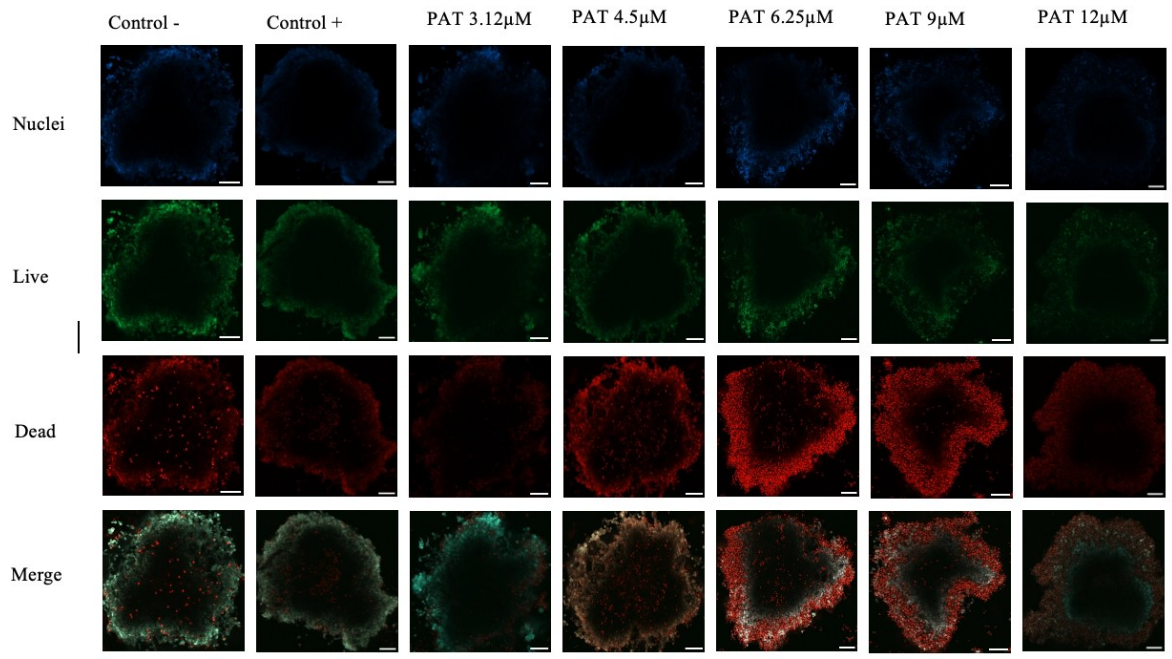

Figure 3.9: *Viability assessment of SH-SY5Y 3D spheroids after 24 hours of exposure to selected concentrations of PAT mycotoxins. Cell's nuclei were staining with Hoechst, live and dead cells were stained using fluorescent calcein-AM and ethidium homodimer-1, respectively (scale bar: 100 µm; objective 10X).*

The figure depicts a qualitative increase in cellular mortality from concentration 4.5 µM to concentration 9 µM, steadily growing. Conversely, concentration 12.5 µM does not exhibit the same mortality, likely due to the dye's limited ability to penetrate the spheroid. Cellular vitality, on the other hand, exhibits a growing trend with increasing PAT concentration in the medium, as observed by the green marker.

3.1.3.2 MTT assay

The latest assay conducted on spheroids to evaluate the cytotoxic effects of toxins is MTT assay. The MTT protocol is available in section §2.5.2. MTT is a quantitative index assay of cellular mortality and complements the qualitative analyses of the Live&Dead.
MTT data related to OTA toxin are presented below.

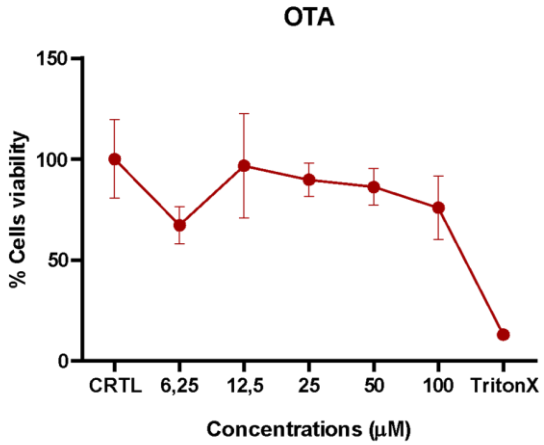

Figure 3.10 *Cell viability trend of SH-SY5Y spheroids quantified by MTT assay, after 24h exposure to OTA.*

The graphical representation of OTA concentration unveils a consistent reduction in vitality with the toxin's increasing levels, particularly noticeable from the concentration of 12.5 µM onward. This marked decline in cellular viability underscores the adverse impact of heightened OTA exposure on cellular health. The graph also depicts a so called hormetic effect, which is a unique dose-response pattern. At the concentration of 6.25 µM, this phenomenon emerges where lower doses paradoxically induce a more substantial response than higher doses. This intriguing hormetic effect is vividly illustrated by a corresponding cellular mortality rate of approximately 65%, providing an insight into the complex dynamics of cellular responses to varying OTA concentrations.

Different effects occur for PAT. The MTT assay (Figure 3.11) is described below.

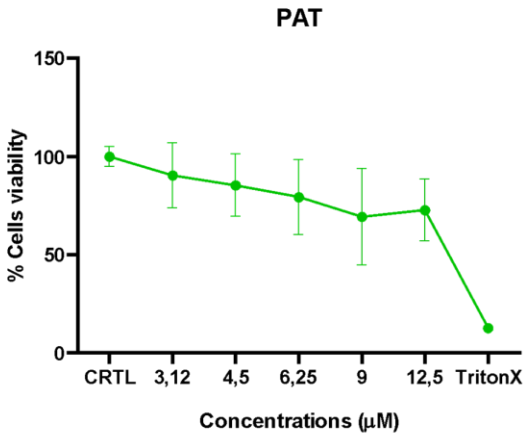

Figure 3.11 *Cell viability trend of SH-SY5Y spheroids quantified by MTT assay, after 24h exposure to PAT.*

The graphical representation of PAT concentration reveals a consistent decline in cellular mortality as the toxin concentration increases, following a linearly decreasing pattern that aligns with intuitive expectations. At concentration 9 µM, cellular mortality reaches

approximately 70%, surpassing that of concentration 12.5 μM, despite marginally. Notably, concentration 9 μM displays a relatively high standard deviation, evident from the associated bar, indicating potential unreliability in the mortality data for this concentration compared to other instances. This variability may be attributed to experimental variability arising from operator-dependent and cell-dependent factors, despite the rigor of repeated trials.

However, it is worth emphasizing that, even with the observed variability, the MTT assay consistently supports the qualitative insights derived from Live&Dead staining. The findings affirm that PAT induces cytotoxic effects on neuroblastoma spheroids after a 24-hour exposure, a phenomenon comparable in magnitude to the effects observed with OTA although through different mechanisms. Regarding PAT, there is a cytotoxicity that is directly proportional to the toxin concentration to which the spheroids are exposed, whereas OTA is more cytotoxic at lower concentrations, a phenomenon explained by hormesis. These findings are applicable to a 24h exposure to the mycotoxin. This concurrence reinforces the reliability and robustness of the overall experimental results.

3.2 Drug testing on 3D CRC spheroids

This section will discuss the results of the experiment conducted with the chip for drug testing on CRC spheroids.

3.2.1 CRC spheroids production and characterization

Colorectal cancer spheroids were produced using the cell line HCT15. Following spheroid production as seen in §2.1.4, characterization was carried out using AnaSP software, detailed in Section §2.3.4. The analysis, as for NB spheroids, focused on parameters such as compactness, sphericity, and Sphericity Index (SI) of the spheroids at days 3, 5, and 7.

Upon completion of the spheroid protocol, cells were observed to cluster without being attached to each other remaining distinguishable with a characteristic round shape indicative of non-attachment.

By day 3, cells had aggregated, forming the spheroid (Figure 3.12 (a)). Subsequent days saw cell growth, enlarging the spheroid and filling empty spaces (Figure 3.12 (b)). Complete spheroid formation is visible after 7 days (Figure 3.12 (c)).

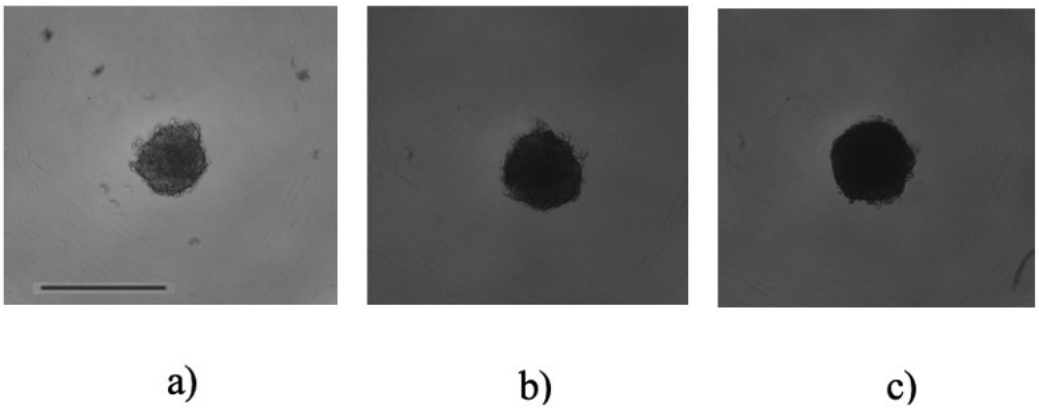

Figure 3.12 *Schematic representation of the process of spheroid's formation:(a) formation of a loose aggregate (b) middle stage of spheroid growth (c) example of spheroid formation derived from SH-SY5Y cells. Scale bar 500 µm; objective 4X.*

This evolution in analysis provides a clearer picture of the morphological changes in the spheroids over time, as shown in the graph below (Figure 3.13). The graph illustrates a subtle yet progressive increase in compactness and solidity. The SI underwent a noticeable increase by day 7, exceeding the desired value of 0.9 shown by the dotted line in the graph and making the spheroids ready for the experiment.

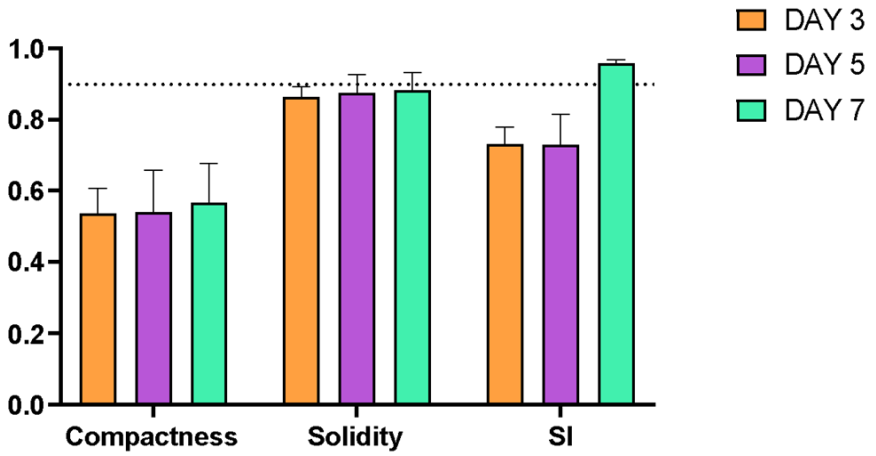

Figure 3.13 *Graph adapted from GraphPad, showing the evolution of spheroid features at days 3, 5 and 7.*

At this stage differences in morphological parameters are noted between the spheroids of SHSY5Y and the spheroids of HCT15. This is due to the diversity of cell line used, and the variability of the operator-dependent experiment.

3.2.2 Platform validation

3.2.2.1 Fluid dynamic validation with colorant and fluorescein isothiocyanate labeled dextrans

Fluid dynamic validation of the platform for drug testing is first performed as in Section §2.4.1.1

The validations verified the creation of five distinct concentrations, with a higher concentration in the left chamber gradually diminishing towards the right (Figure 3.14). Additionally, steady-state conditions were sustained for several hours.

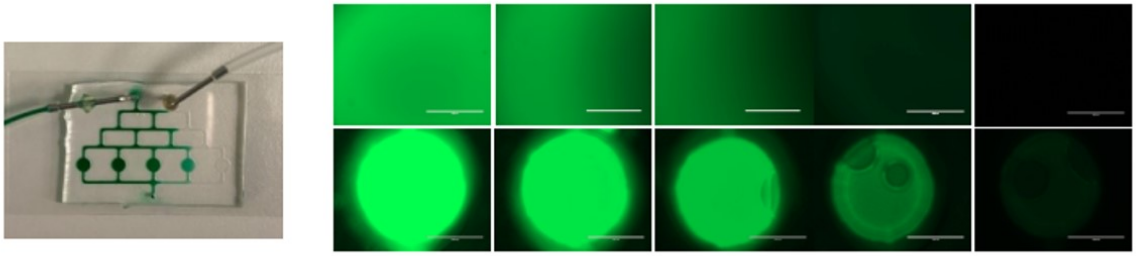

a) b)

Figure 3.14 *Validation with green colorant (a) and fluorescein isothiocyanate labeled dextran (b). Scale bar 1000 µm.*

3.2.2.2 Fluid dynamic validation with COMSOL Multiphysics

Validation continues through COMSOL as described in section §2.4.1.2. From the simulations, the lowest flow rate which allows to reach the steady state in 1 hour is 2 µL/min and the results are represented in Figures 3.15, 3.16.

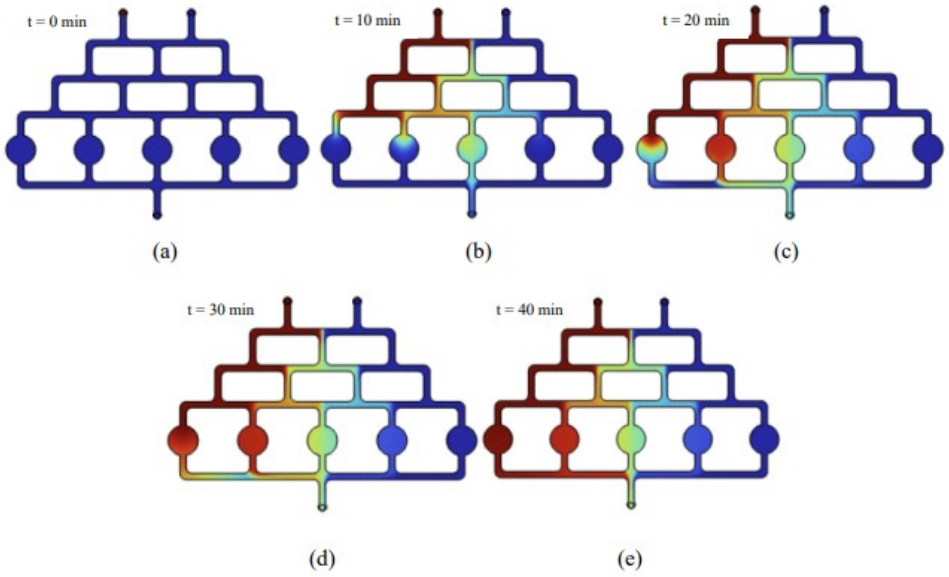

Figure 3.15 *Fluid dynamic simulation of the multi-concentration drug delivery system geometry. At time 0 minutes (a), after 10 minutes (b), 20 minutes (c), 30 minutes (d) and 40 minutes (e).*

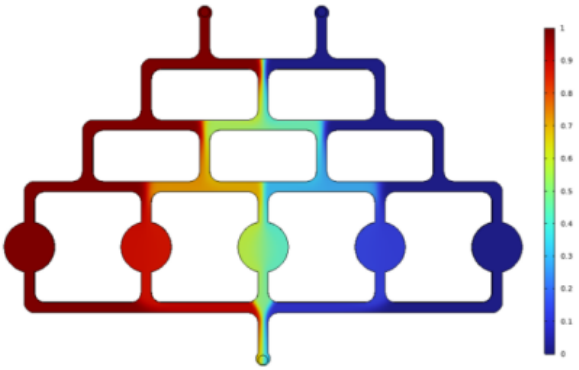

Figure 3.16 *Steady state concentration heatmap from the fluid dynamic simulation of the multi-concentration drug delivery system.*

The validations confirm the establishment of 5 different concentrations, with a higher concentration in the left chamber and a gradual decrease of the concentration moving to the right. Also in this case, the steady state is maintained for several hours.

3.2.2.3 Biological validation

The device is biologically validated as described in §2.4.2.
The device is considered validated if the spheroid configuration remains stable upon seeding within the platform, crucial for preventing rupture or deformation during subsequent medium flow (Figure 3.17).

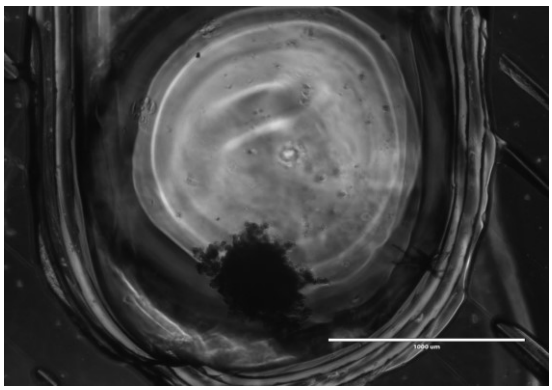

Figure 3.17 *HCT-15 spheroids seeded on chip with GelMA (t=0). Scale bar 1000 µm.*

The double-layer chip configuration enables the spheroids to rest in the bottom layer, allowing medium flow without direct exposure. To ensure the health of the spheroids within the chip, a Live&Dead assay is performed. Figure 3.18 illustrates the success of the biological validation, with most cells stained green, indicating their viability.

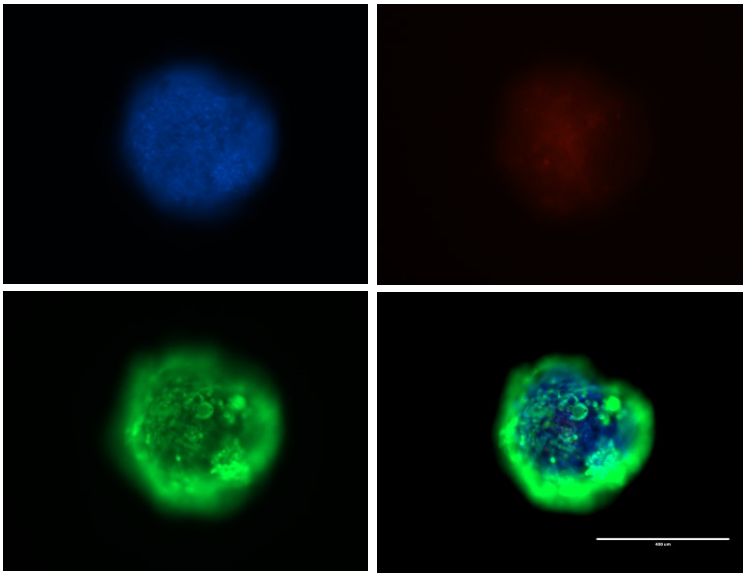

Figure 3.18 *Live and dead assay of HCT-15 spheroids after 72h of medium exposure in the microfluidic chip at flow rate of 1µl/min. Scale bar 1000 µm.*

3.2.3 Drug testing

3.2.3.1 Live&Dead assay

The Live&Dead assay evaluates the cell viability of spheroids after 72 hours of 5FU exposure. Figure 3.19 illustrates spheroids in the microfluidic platform, arranged from the highest (100% 5FU) to zero concentration (0% 5FU). The leftmost well, receiving only 5FU, exhibits significantly higher mortality, indicated by a brighter red color. Mortality decreases moving right, nearly reaching zero in the well with only medium. Concurrently, viability, represented in green, increases from the highest drug concentration to its maximum in the well with only medium. These results indicate that 5FU, under these conditions, adversely affects NB spheroids, with higher concentrations showing increased harm.

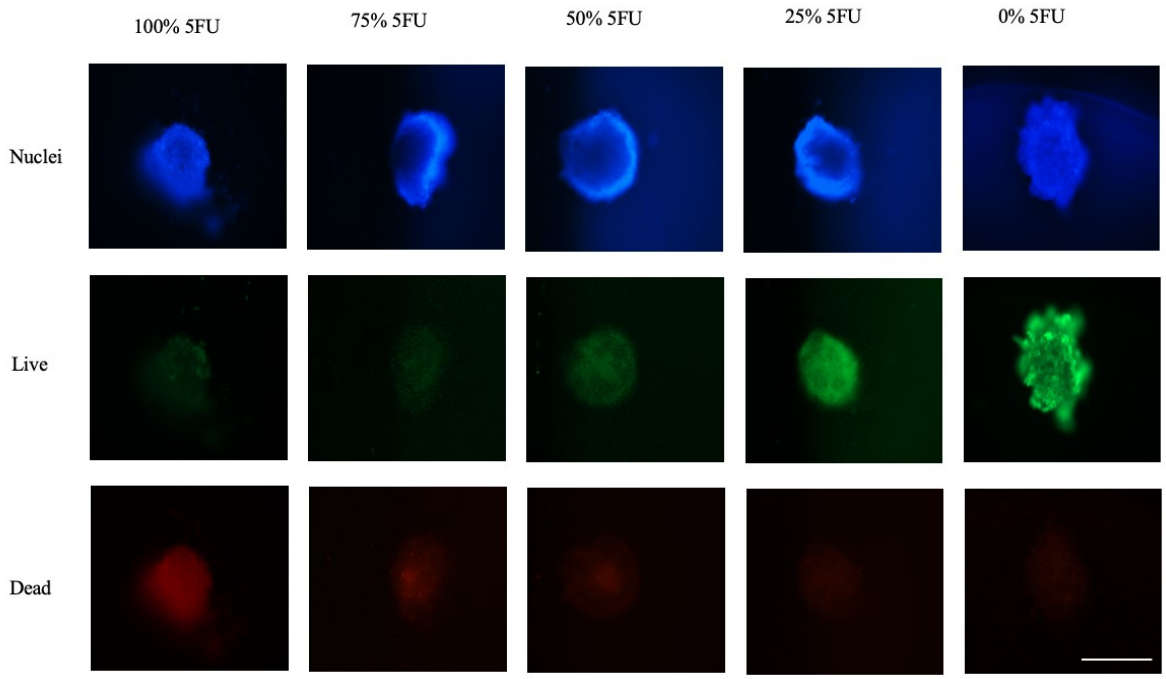

Figure 3.19 *Viability assessment of HCT15 3D spheroids after 72 hours of exposure to5FU. Cell's nuclei were staining with Hoechst, live and dead cells were stained using fluorescent calcein-AM and propidium iodide, respectively. Scale bar 1000 µm.*

Conclusions

In conclusion, this thesis project successfully develops innovative strategies for conducting toxicological studies using microfluidics, addressing the challenge of evaluating cytotoxic effects induced by mycotoxins on NB spheroids and drug testing on CRC spheroids.
Microfluidic systems hold the potential to revolutionize the field of toxicology and drug discovery, enabling the testing of compounds on cells or spheroids, and utilizing minimal volumes of reagents.

The SFD chip designed for the cytotoxic evaluation of mycotoxins is manufactured through soft lithography techniques, produced using PDMS and validated using colorant tracers and SHSY5Y spheroids. The mycotoxins employed in this toxicological study are OTA and PAT, both food toxins introduced into the human body through the diet. Through qualitative (Live&Dead) and quantitative (MTT) assays we demonstrate that after 24 hours of exposure to OTA and PAT individually, a significant portion of the cells constituting the SHSY5Y spheroid undergoes cell death, confirming the cytotoxic effects of mycotoxins.

The MGG chip designed for drug testing is conceived using COMSOL Multiphysics® modeling software, enabling the exploration of fluid dynamics, gradient formation, and concentration profiles within the microfluidic system. The master mold is created using photolithography, and the PDMS microfluidic chip is obtained through replica molding processes. This configuration of the platform is used for both fluid dynamic validations, employing different colored tracers, and biological validations, using HCT15 spheroids. Fluid dynamic validation confirmed the attainment of the derived concentration gradient.
Spheroids are exposed to 72h of 5FU (5 Fluorouracyl), a chemotherapeutic drug, at the different concentrations created by the microfluidic device. Viability assays conducted shows that 5FU was cytotoxic at most when present in high concentrations.

Overall, the versatility and efficiency of the microfluidic device make it a unique tool for conducting toxicological studies. By providing controlled environments for mycotoxin exposure and drug gradient generation, the devices facilitate precise assessment of toxic compound effects on biological systems, contributing to advancements in the field.

References

1. Squires TM, Quake SR. *Microfluidics: Fluid Physics at the Nanoliter Scale*.
2. Sackmann EK, Fulton AL, Beebe DJ. The present and future role of microfluidics in biomedical research. *Nature*. 2014;507(7491):181-189. doi:10.1038/nature13118
3. Yeo LY, Chang HC, Chan PPY, Friend JR. Microfluidic devices for bioapplications. *Small*. 2011;7(1):12-48. doi:10.1002/smll.201000946
4. Dittrich PS, Manz A. Lab-on-a-chip: Microfluidics in drug discovery. *Nat Rev Drug Discov*. 2006;5(3):210-218. doi:10.1038/nrd1985
5. Breslauer DN, Lee PJ, Lee LP. Microfluidics-based systems biology. *Mol Biosyst*. 2006;2(2):97-112. doi:10.1039/b515632g
6. Ren K, Zhou J, Wu H. Materials for microfluidic chip fabrication. *Acc Chem Res*. 2013;46(11):2396-2406. doi:10.1021/ar300314s
7. Nge PN, Rogers CI, Woolley AT. Advances in microfluidic materials, functions, integration, and applications. *Chem Rev*. 2013;113(4):2550-2583. doi:10.1021/cr300337x
8. *Materials for Microfluidic Chips Fabrication : A Review 2017-Elveflow Https://Www.Elveflow.Com/Microfluidic-Reviews/General-Microfluidics/Materials-for-Microfluidic-Chips-Fabrication-a-Review-2017/ Materials for Microfluidic Chips Fabrication: A Review*. https://www.elveflow.com/microfluidic-reviews/general-microfluidics/materials-for-microfluidic-chips-fabrication-a-review-2017/
9. *PDMS: A Review on Polydimethylsiloxane in Microfluidics-Elveflow PDMS: A Review Introduction to Polydimethylsiloxane*. https://www.elveflow.com/microfluidic-reviews/general-microfluidics/the-polydimethylsiloxane-pdms-and-microfluidics/
10. Regehr KJ, Domenech M, Koepsel JT, et al. Biological implications of polydimethylsiloxane-based microfluidic cell culture. *Lab Chip*. 2009;9(15):2132-2139. doi:10.1039/b903043c
11. Tung Nguyen Hoang. *Photolithography*. http://public.itrs.net.
12. Becker H, Gärtner C. Polymer microfabrication technologies for microfluidic systems. *Anal Bioanal Chem*. 2008;390(1):89-111. doi:10.1007/s00216-007-1692-2
13. Whitesides GM, Ostuni E, Takayama S, Jiang X, Ingber DE. *SOFT LITHOGRAPHY IN BIOLOGY AND BIOCHEMISTRY*.; 2001. www.annualreviews.org

14. Weibel DB, DiLuzio WR, Whitesides GM. Microfabrication meets microbiology. *Nat Rev Microbiol*. 2007;5(3):209-218. doi:10.1038/nrmicro1616
15. Zhou J, Ellis AV, Voelcker NH. Recent developments in PDMS surface modification for microfluidic devices. *Electrophoresis*. 2010;31(1):2-16. doi:10.1002/elps.200900475
16. Bargahi N, Ghasemali S, Jahandar-Lashaki S, Nazari A. Recent advances for cancer detection and treatment by microfluidic technology, review and update. *Biol Proced Online*. 2022;24(1). doi:10.1186/s12575-022-00166-y
17. Davidoff AM, Fernandez-Pineda I, Santana VM, Shochat SJ. The role of neoadjuvant chemotherapy in children with malignant solid tumors. *Semin Pediatr Surg*. 2012;21(1):88-99. doi:10.1053/j.sempedsurg.2011.10.010
18. Maris JM. *Philadel-Phia, PA 19104-4318 or at Maris@chop .Edu*. Vol 3060.; 2010. www.ncbi.nlm.nih.gov/
19. Favoriti P, Carbone G, Greco M, Pirozzi F, Pirozzi REM, Corcione F. Worldwide burden of colorectal cancer: a review. *Updates Surg*. 2016;68(1):7-11. doi:10.1007/s13304-016-0359-y
20. Alzahrani SM, Al Doghaither HA, Al-Ghafar AB. General insight into cancer: An overview of colorectal cancer (review). *Mol Clin Oncol*. 2021;15(6). doi:10.3892/MCO.2021.2433
21. Arvelo F, Sojo F, Cotte C. Biology of colorectal cancer. *Ecancermedicalscience*. 2015;9. doi:10.3332/ecancer.2015.520
22. Edmondson R, Broglie JJ, Adcock AF, Yang L. Three-dimensional cell culture systems and their applications in drug discovery and cell-based biosensors. *Assay Drug Dev Technol*. 2014;12(4):207-218. doi:10.1089/adt.2014.573
23. Robinson NB, Krieger K, Khan F, et al. The current state of animal models in research: A review. *International Journal of Surgery*. 2019;72:9-13. doi:10.1016/j.ijsu.2019.10.015
24. DIRETTIVA UE DEL PARLAMENTO EUROPEO E DEL CONSIGLIO.
25. Hirschhaeuser F, Menne H, Dittfeld C, West J, Mueller-Klieser W, Kunz-Schughart LA. Multicellular tumor spheroids: An underestimated tool is catching up again. *J Biotechnol*. 2010;148(1):3-15. doi:10.1016/j.jbiotec.2010.01.012
26. Han SJ, Kwon S, Kim KS. Challenges of applying multicellular tumor spheroids in preclinical phase. *Cancer Cell Int*. 2021;21(1). doi:10.1186/s12935-021-01853-8

27. Achilli TM, Meyer J, Morgan JR. Advances in the formation, use and understanding of multi-cellular spheroids. *Expert Opin Biol Ther*. 2012;12(10):1347-1360. doi:10.1517/14712598.2012.707181
28. Huang L, Abdalla AME, Xiao L, Yang G. Biopolymer-based microcarriers for three-dimensional cell culture and engineered tissue formation. *Int J Mol Sci*. 2020;21(5). doi:10.3390/ijms21051895
29. Bartosh TJ, Ylostalo JH. Preparation of anti-inflammatory mesenchymal stem/precursor cells (MSCs) through sphere formation using hanging-drop culture technique. *Curr Protoc Stem Cell Biol*. 2014;1(SUPPL.28). doi:10.1002/9780470151808.sc02b06s28
30. Lewis NS, Lewis EEL, Mullin M, Wheadon H, Dalby MJ, Berry CC. Magnetically levitated mesenchymal stem cell spheroids cultured with a collagen gel maintain phenotype and quiescence. *J Tissue Eng*. 2017;8. doi:10.1177/2041731417704428
31. Ryu NE, Lee SH, Park H. Spheroid culture system methods and applications for mesenchymal stem cells. *Cells*. 2019;8(12). doi:10.3390/cells8121620
32. Zingales V, Torriero N, Zanella L, et al. Development of an in vitro neuroblastoma 3D model and its application for sterigmatocystin-induced cytotoxicity testing. *Food and Chemical Toxicology*. 2021;157. doi:10.1016/j.fct.2021.112605
33. Booij TH, Price LS, Danen EHJ. 3D Cell-Based Assays for Drug Screens: Challenges in Imaging, Image Analysis, and High-Content Analysis. *SLAS Discovery*. 2019;24(6):615-627. doi:10.1177/2472555219830087
34. Bennett JW. *Mycotoxins, Mycotoxicoses, Mycotoxicology and Mycopathologia*. Vol 100.; 1987.
35. Hussein HS, Brasel JM. *Toxicity, Metabolism, and Impact of Mycotoxins on Humans and Animals*. Vol 167.; 2001. www.elsevier.com/locate/toxicol
36. Council for Agricultural Science and Technology. *Mycotoxins : Risks in Plant, Animal, and Human Systems.* Council for Agricultural Science and Technology; 2003.
37. *Alert and Cooperation Network Health and Food Safety*.
38. Malir F, Pickova D, Toman J, Grosse Y, Ostry V. Hazard characterisation for significant mycotoxins in food. *Mycotoxin Res*. 2023;39(2):81-93. doi:10.1007/s12550-023-00478-2
39. IARC Working Group on the Evaluation of Carcinogenic Risks to Humans., International Agency for Research on Cancer. *Some Naturally Occurring Substances : Food Items and Constituents, Heterocyclic Aromatic Amines and Mycotoxins.* World Health Organization, International Agency for Research on Cancer; 1993.

40. Schrenk D, Bodin L, Chipman JK, et al. Risk assessment of ochratoxin A in food. *EFSA Journal*. 2020;18(5). doi:10.2903/j.efsa.2020.6113
41. *List of Classifications-IARC Monographs on the Identification of Carcinogenic Hazards to Humans*.
42. Patulin in the common cold collaborative research.
43. Tannous J, Keller NP, Atoui A, et al. Secondary metabolism in Penicillium expansum: Emphasis on recent advances in patulin research. *Crit Rev Food Sci Nutr*. 2018;58(12):2082-2098. doi:10.1080/10408398.2017.1305945
44. Saleh I, Goktepe I. The characteristics, occurrence, and toxicological effects of patulin. *Food and Chemical Toxicology*. 2019;129:301-311. doi:10.1016/j.fct.2019.04.036
45. Pal S, Singh N, Ansari KM. Toxicological effects of patulin mycotoxin on the mammalian system: An overview. *Toxicol Res (Camb)*. 2017;6(6):764-771. doi:10.1039/c7tx00138j
46. Askr H, Elgeldawi E, Aboul Ella H, Elshaier YAMM, Gomaa MM, Hassanien AE. Deep learning in drug discovery: an integrative review and future challenges. *Artif Intell Rev*. 2023;56(7):5975-6037. doi:10.1007/s10462-022-10306-1
47. Mohs RC, Greig NH. Drug discovery and development: Role of basic biological research. *Alzheimer's and Dementia: Translational Research and Clinical Interventions*. 2017;3(4):651-657. doi:10.1016/j.trci.2017.10.005
48. Wigmore PM, Raffa RB, Tallarida RJ, et al. *Chapter 20 Effects of 5-FU*.
49. *SH-SY5Y*. https://www.atcc.org/products/crl-2266
50. *HCT-15 CCL-225*. https://www.atcc.org/products/ccl-225
51. Booij TH, Price LS, Danen EHJ. 3D Cell-Based Assays for Drug Screens: Challenges in Imaging, Image Analysis, and High-Content Analysis. *SLAS Discovery*. 2019;24(6):615-627. doi:10.1177/2472555219830087
52. Tsai PJ, Lee IC, Yen MH, Ethan Li YC. Development and customization of a concentration gradient microgenerator by extrusion 3D printing for drug testing in laboratory studies. *Bioprinting*. 2021;23. doi:10.1016/j.bprint.2021.e00160 52
53. Gungor-Ozkerim PS, Inci I, Zhang YS, Khademhosseini A, Dokmeci MR. Bioinks for 3D bioprinting: An overview. *Biomater Sci*. 2018;6(5):915-946. doi:10.1039/c7bm00765e 53
54. Zingales V, Torriero N, Zanella L, et al. Development of an in vitro neuroblastoma 3D model and its application for sterigmatocystin-induced cytotoxicity testing. *Food and Chemical Toxicology*. 2021;157. doi:10.1016/j.fct.2021.112605 54